Copyright Warning & Restrictions

The copyright law of the United States (Title 17, United States Code) governs the making of photocopies or other reproductions of copyrighted material.

Under certain conditions specified in the law, libraries and archives are authorized to furnish a photocopy or other reproduction. One of these specified conditions is that the photocopy or reproduction is not to be "used for any purpose other than private study, scholarship, or research." If a, user makes a request for, or later uses, a photocopy or reproduction for purposes in excess of "fair use" that user may be liable for copyright infringement,

This institution reserves the right to refuse to accept a copying order if, in its judgment, fulfillment of the order would involve violation of copyright law.

Please Note: The author retains the copyright while the New Jersey Institute of Technology reserves the right to distribute this thesis or dissertation

Printing note: If you do not wish to print this page, then select "Pages from: first page # to: last page #" on the print dialog screen

ABSTRACT

MICROENGINEERED MASS SPECTROMETER WITH FIELD EMISSION IONIZATION SOURCE

by
Chao Sun

This thesis describes a design for a microengineered mass spectrometer. This mass spectrometer device uses VLSI processing techniques to scale down the dimensions of an existing mass spectrometer and make it portable. It can be manufactured economically and has the potential to be integrated with more complex structures and including transistor integrated circuits. An optimized device is proposed. This device is to be fabricated using two silicon substrates approximately 1cm by 1cm, where one is a cathode electron source and the other is the ion collector. External ion sources are not needed. Electrons are emitted from the array of cathode tips by field emission. Gas molecules near the cathode are bombarded by electrons and ionized. An electrostatic field and a uniform magnetic field of 3000 Gauss are used to establish separate trajectories for each mass isotope. Each mass isotope ion is collected at a different location on the ion collector plane. Voltage supply levels are 0 and 50V. The 3000 Gauss magnetic field permits collection of ions of up to 222amu (radon) for the spatial dimensions selected for this design Analyses of electron and ion trajectories were carried out using the SIMION simulation program. Many different structures were simulated and the optimized geometry of the microengineered mass spectrometer was determined. Sensitivities of the device have been modeled and calculated for the molecular range up to 222amu. The minimum detectable density level for an isotope is proportional to the active ionizing volume and is limited by the input noise level of the ion collection detector circuits. Fabrication procedures are detailed in this thesis.

MICROENGINEERED MASS SPECTROMETER WITH FIELD EMISSION IONIZATION SOURCE

by
Chao Sun

A Thesis
Submitted to the Faculty of
New Jersey Institute of Technology
in Partial Fulfillment of the Requirements for the Degree of
Master of Science in Electrical Engineering

Department of Electrical and Computer Engineering

May 1993

APPROVAL PAGE

Microengineered Mass Spectrometer with Field Emission Ionization Source

Chao Sun

5-12-93

Dr. William N. Carr, Thesis Adviser (date)
Professor and Holder of Sponsored Chair in Microelectronics, NJIT

5/7/93

Dr. M Anandan, Committee Member (date)
Thomas Electronics, Inc , Wayne, NJ

5/7/93

Dr. Kenneth R. Farmer, Committee Member (date)
Assistant Professor of Physics, NJIT

5/7/93

Dr Robert B Marcus, Committee Member (date)
Distinguished Professor of Physics and Chemical Engineering, NJIT

5/7/93

Dr. Shi Chang Wu, Committee Member (date)
Assistant Professor of Electrical Engineering, NJIT

BIOGRAPHICAL SKETCH

Author: Chao Sun

Degree: Master of Science in Electrical and Computer Engineering

Date: May 1993

Date of Birth:

Place of Birth:

Undergraduate and Graduate Education:

- Master of Science in Electrical Engineering,
  New Jersey Institute of Technology, Newark, NJ, USA, 1993
- Bachelor of Science in Physics,
  Fudan University, Shanghai, P. R China, 1982

Major: Electrical Engineering

This thesis is dedicated to
my wife and my parents

ACKNOWLEDGMENT

I would like to express my sincere gratitude to my advisor Professor William N. Carr for his valuable guidance, consistent support and encouragement.

I would also like to thank the members of my thesis committee Dr. M. Anandan, Dr. Kenneth R. Farmer, Dr. Robert B. Marcus, and Dr. Shi Chang Wu. I have benefited significantly from the suggestions made by them.

I am greatly indebted to my wife and my parents for their moral support and encouragement.

TABLE OF CONTENTS

LIST OF TABLES

LIST OF FIGURES

Figure **Page**

Figure **Page**

CHAPTER ONE
INTRODUCTION

There is a growing interest worldwide in the concept and possible applications of miniature, micro and even nanoscale devices. This thesis describes an design for a microengineered mass spectrometer based on field emission cathodes for ionization. The dimension of this device is approximately 1cm. VLSI processing techniques can be used for device fabrication.

Chapter two includes the basic principles of a mass spectrometer and its characterization. Some important properties and design equations are developed and discussed. The device modeling in later chapters is based on these equations.

Chapter three describes the features of this microengineered mass spectrometer device. Several different design structures for this device with the electron and ion trajectories are shown. Advantages and disadvantages of each structure are discussed. The optimized design is determined.

Chapter four discusses the critical design structure in this device, the cathodes. Sensitivity and some other important parameters of the optimized design are modeled and calculated.

The process methodology is presented in chapter five. Detailed fabrication process steps for the device including mask design are illustrated.

Chapter six describes the testing circuit testing environment.

CHAPTER TWO
MASS SPECTROMETER BASIC PRINCIPLES

Mass spectrometers are used to measure the ratio of mass to electric charge of a molecule or atom. There are several forms of mass spectrometer but the basic principle of operation is common: first the gas molecules are ionized, then accelerated and separated into groups according to their mass-to-charge values, and finally detected. See Figure 2.1.

The means of ionization are fairly standard, the gas molecules being bombarded by electrons. The acceleration is done by electric fields, while the separation is done by using magnetic deflection, resonance or time of flight techniques. A variety of methods has been developed for each of the three stages of particle identification. Other methods have been developed into portable instruments. This chapter reviews briefly the basic principles of the commonly used ionization, separation, and detection methods in mass spectrometer. The basic concepts of vacuum and gas pressure parameters necessary for this design are developed in this chapter.

2.1 Basic Concepts of Vacuum and Gas Pressure

A gaseous environment where pressure or density is below that of standard atmosphere is termed a vacuum. The physical quantity used to characterize such an environment is the gas pressure. Usually vacuum is obtained by removing gas from an airtight vessel by some means of pumping. In the absence of a gas load, the degree of vacuum in the vessel increases as the pressure of the residual gases decreases.

Generally speaking, pressure is a convenient parameter to characterize vacuum. However, below certain limits of gas rarefaction, pressure is not adequate to explain phenomena that take place in the vacuum, and other physical

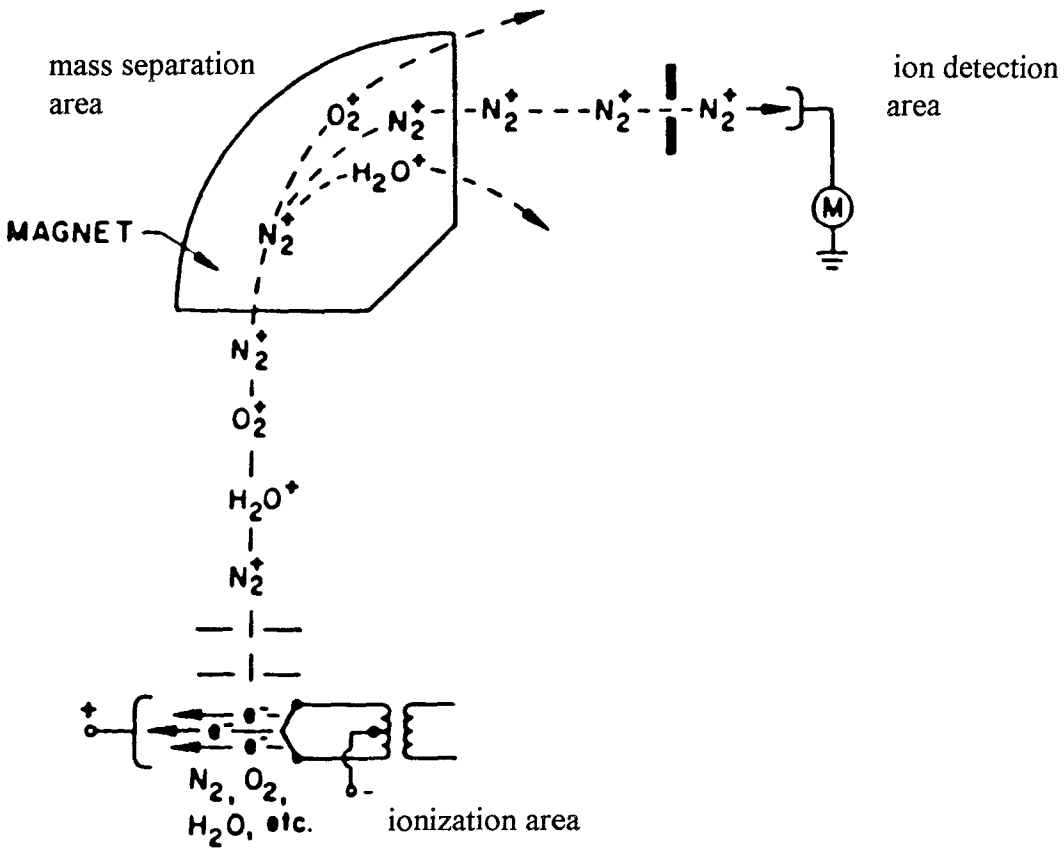

Figure 2.1 Functional drawing of a mass spectrometer shows ionization area, mass separation area, and ion detection area.

quantities, such as the density of molecules and the mean free path, can characterize it more exactly. The meaning and magnitude of these quantities is given by the kinetic theory of gases. According to this theory, a gas is a collection of an enormous number of particles (molecules) moving along random directions, colliding with each other, and changing their direction of motion with each collision. For a gas sample of mass M, having a known absolute temperature T, and molecular weight m, the product of the pressure P and volume V is given by

$$PV = \frac{M}{m}RT \tag{2.1}$$

where M/m is the number of moles and R is an universal constant, $R = 62.36$ Torr·liter / K·mole Equation (2.1) is the general gas law. The number of molecules n per unit volume is

$$n = \frac{M}{m} \cdot \frac{N_A}{V} \tag{2.2}$$

where N_A is the Avogadro's number, $N_A = 6.023 \times 10^{23}$ molec./mole.

From equations (2.1) and (2.2), n becomes

$$n = \frac{N_A P}{RT}. \tag{2.3}$$

If P is expressed in Torr, and R in Torr·cm^3/K, the number of molecules per cm^3 is given by

$$n = \frac{6.023 \times 10^{23}}{6.236 \times 10^4} \cdot \frac{P}{T} = 9\ 656 \times 10^{18} \cdot \frac{P}{T} \quad (cm^{-3}). \tag{2.4}$$

Equation (2.3) can also be written

$$P = n \cdot \frac{R}{N_A} \cdot T = nkT \tag{2.5}$$

where k is the Boltzmann constant and expressed as $k=R/N_A=1.035\times10^{-22}$ Torr·liter/K·mole.

Gas molecules collide with each other. These collisions produce a distribution of velocities. Maxwell and Boltzmann expressed the distribution of the velocities by the relationship [2]

$$\frac{1}{n}\frac{dn}{dv} = f_v = \frac{4}{\pi^{1/2}}\left(\frac{m}{2kT}\right)^{3/2} v^2 \exp\left(\frac{-mv^2}{2kT}\right) \tag{2.6}$$

where f_v is the fractional number of molecules in the velocity range between v and v+dv, per unit of velocity range, and m is the mass of molecule. The distribution function of the velocities of molecules in the x direction was written as

$$\frac{1}{n}\frac{dn_x}{dv_x} = f_{v_x} = \left(\frac{m}{2\pi kT}\right)^{1/2} \exp\left(\frac{-mv_x^2}{2kT}\right). \tag{2.7}$$

The number of molecules striking a unit area of surface (perpendicular to the x direction), per unit time is given by

$$\phi = \int_0^\infty v_x dn_x. \tag{2.8}$$

The symbol ϕ is the incident flux density rate. By introducing dn_x from equation (2.7) into (2.8) and integrating, it results that

$$\phi = \frac{n}{2\pi^{1/2}}\left(\frac{2kT}{m}\right)^{1/2} \tag{2.9}$$

By using equation (2.4), the incident flux density rate ϕ becomes

$$\phi = 3.513\times10^{22}\cdot\frac{P}{(mT)^{1/2}} \quad (\text{molec./cm}^2\text{s}) \tag{2.10}$$

where P is in Torr, m is the molecular weight of the gas and T is the absolute temperature.

The average distance traversed by a molecule between successive collisions is its mean free path λ. A molecule having a diameter δ and a velocity v moves at

a distance v·dt in the time dt The molecule suffers a collision with another molecule when its center is within the distance δ of the center of another molecule, therefore sweeps out without collision a cylinder of diameter 2δ. This cylinder has a volume

$$dV = \frac{\pi}{4}(2\delta)^2 v dt. \tag{2.11}$$

Since there are n molecules per cm^3, the volume associated with one molecule is on the average $1/n$ cm^3. When the volume dV is equal to 1/n, it must contain on the average one other molecule, thus a collision has occurred. If τ=dt is the average time between collisions,

$$\frac{1}{n} = \pi\delta^2 v\tau \tag{2.12}$$

and the mean free path λ is

$$\lambda = v\tau = \frac{1}{\pi n\delta^2}. \tag{2.13}$$

If we consider the more realistic case, in which not only the reference molecule is in motion but also the others, then equation (2.13) must be written

$$\lambda = \frac{1}{\pi n\delta^2}\cdot\frac{v}{v_r} \tag{2.14}$$

where v is the absolute velocity, while v_r is relative velocity of the molecules. When the Maxwell-Boltzmann distribution of velocities is also considered, it results that

$$\frac{v}{v_r} = \frac{1}{\sqrt{2}} \tag{2.15}$$

$$\lambda = \frac{1}{\sqrt{2}\pi n\delta^2}. \tag{2.16}$$

By using equation (2.4), λ becomes

$$\lambda = 2.33 \times 10^{-20} \cdot \frac{T}{\delta^2 P} \quad (cm) \tag{2.17}$$

where T is in K, δ in cm, and P in Torr.

Figure 2.2 illustrates the variation of the quantities expressed by Equations (2.4), (2.10), and (2.17) in different vacuum ranges. The calculated values of n, ϕ, and λ are shown in Table 2.1. These parameters are used to calculate the sensitivity of the microengineered mass spectrometer device in chapter four.

2.2 Magnetic Deflection Mass Spectrometers

The semicircular, homogeneous field design was first reported by Dempster; and it is still widely employed either as a single magnetic analyzer, or in conjunction with electrostatic lenses. Typical ion trajectories for the 180° magnet arrangement are shown in Figure 2.3, assuming a highly collimated ion beam.

Let singly charged ions be produced and accelerated through a potential V_c, thus acquiring a kinetic energy of magnitude eV_c. If this accelerating potential V_c is large compared with the initial energy distribution of the ions, we can assume that all ions enter the magnetic field with a discrete velocity which is given by

$$eV_c = \frac{1}{2}mv^2, \text{ or } v = \sqrt{\frac{2eV_c}{m}} \tag{2.18}$$

where m is the mass of the ion, e is the electronic charge, and v is the velocity of the ion after acceleration. For positive ions having a charge state ζ (ζ=1,2,3...), where ζ denotes the number of electrons stripped from a neutral atom, the more general expression results

$$\zeta eV_c = \frac{1}{2}mv^2. \tag{2.19}$$

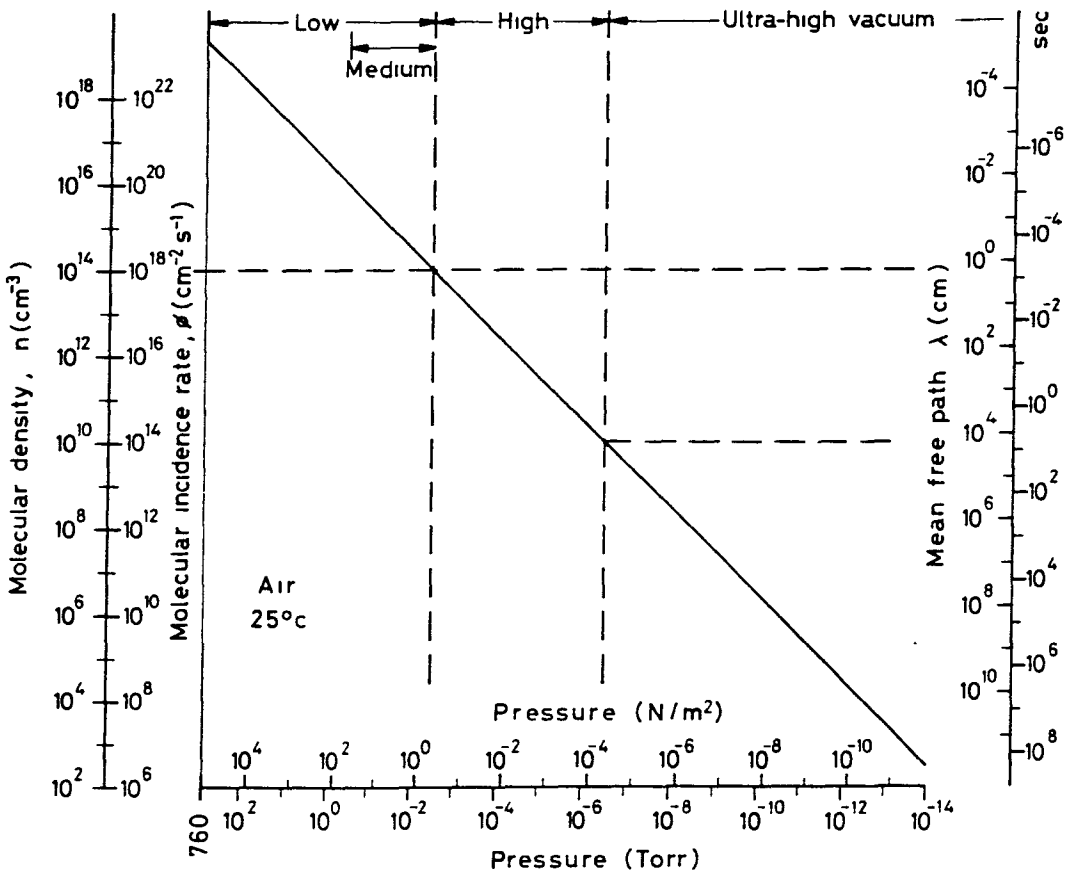

Figure 2.2 Variation of the number density of molecules n, mean free path λ, and molecular incidence rate ϕ as a function of pressure P [2].

Table 2.1(a) Values of molecular density n, molecular incidence rate ϕ, and mean free path λ, as a function of pressure P, for air at 25°C [2].

P Torr	n molec/cm^3	ϕ molec/cm^2·sec	λ cm
760	2.46×10^{19}	2.88×10^{23}	6.7×10^{-6}
1	3.25×10^{16}	3.78×10^{20}	5.1×10^{-3}
10^{-3}	3.25×10^{13}	3.78×10^{17}	5.1
10^{-6}	3.25×10^{10}	3.78×10^{14}	5.1×10^{3}
10^{-9}	3.25×10^{7}	3.78×10^{11}	5.1×10^{6}
10^{-12}	3.25×10^{4}	3.78×10^{8}	5.1×10^{9}
10^{-15}	3.25×10	3.78×10^{5}	5.1×10^{12}

Table 2.1(b) Values of ϕ, and λ for various gases at 25°C and 10^{-3} Torr [2].

Gas	ϕ molec/cm^2·sec	λ cm
H_2	14.4×10^{17}	9.3
He	10.4×10^{17}	14.7
N_2	3.85×10^{17}	5.0
O_2	3.60×10^{17}	5.4
A	3.22×10^{17}	5.3
Air	3.78×10^{17}	5.1
H_2O	4.80×10^{17}	3.4
CO_2	3.07×10^{17}	3.3

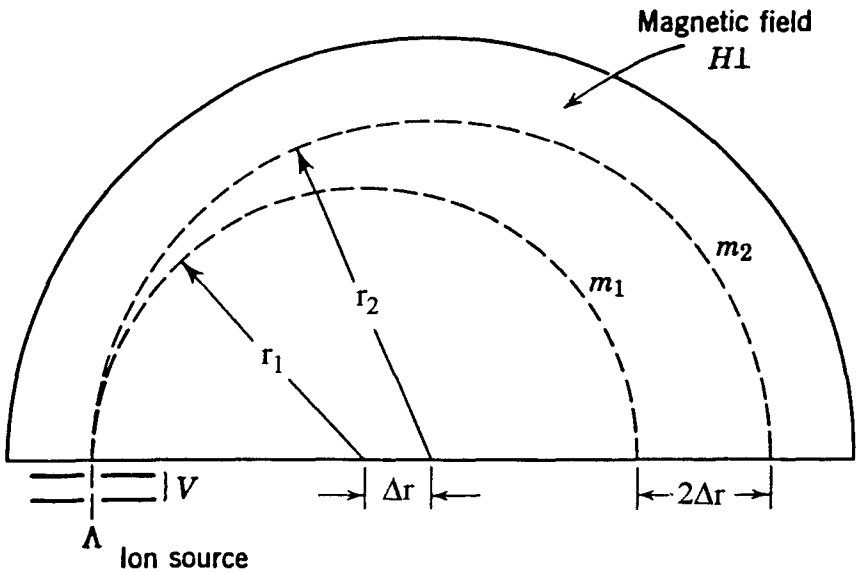

Figure 2.3 Ion paths in a homogeneous 180° magnetic sector.

If the magnetic field B is perpendicular to the velocity vector of the ions, the ions will be deflected into a circular orbit with radius r, resulting from the balancing of centrifuge force with the Lorentz force $B\zeta ev$

$$B\zeta ev = \frac{mv^2}{r}. \tag{2.20}$$

Eliminating v from the above two equations yields the general expression relating the radius of curvature of an ion in a homogeneous magnetic field to the several other parameters:

$$r = \frac{1}{B}\left(\frac{2mV_c}{\zeta e}\right)^{1/2}. \tag{2.21}$$

If the magnetic field strength B is expressed in Gauss, m is given in atomic mass units, V_c is the accelerating potential in volts, and ζ is the multiplicity of

electronic charge, then the radius of curvature r, in centimeters, is approximated by the relation

$$r = \frac{144}{B}\left(\frac{mV_c}{\zeta}\right)^{1/2}. \tag{2.22}$$

The above suggests that for ions accelerated through the same potential, those of large mass number will have a larger radius of curvature. It will also be noted that an ambiguity remains with respect to the mass number and charge state. A doubly-charged magnesium ion of mass 24 Mg^{24} will have approximately the same radius of curvature as will a carbon C^{12} atom that is only singly ionized. Therefore, unless the magnetic analyzer can resolve the small momentum difference corresponding to these two species, only a single peak will be observed at the mass-equals-12 spectral position. The equation can also be differentiated to yield an expression of the general form

$$\frac{2\Delta r}{r} = \frac{\Delta m}{m} + \frac{\Delta V_c}{V_c} - \frac{2\Delta B}{B}. \tag{2.23}$$

For a homogeneous magnetic field and ions having a negligible energy spread, the last two terms will vanish and the equation (2.23) reduces to

$$2\Delta r = \frac{\Delta m}{m} r. \tag{2.24}$$

The quantity $2\Delta r$ gives a measure of the mass dispersion, or the separation of resolved ions along the focal plane. Thus, in Figure 2.3, if r_1 and r_2 are the radii of curvature of masses m_1 and m_2, respectively, the mass dispersion of these two isotopes will result in diameter different

$$2(r_1 - r_2) = \left(\frac{m_1 - m_2}{m_1}\right) r_1 \tag{2.25}$$

For isotopes that differ by only one mass number ($\Delta m=1$), the mass dispersion D along the focal plane will have a magnitude

$$D = c\frac{r}{m} \tag{2.26}$$

where the unitless constant c will depend upon the magnetic sector angle. For the 180° sector, c will be 1, and

$$D = 2\Delta r = \frac{r}{m} \tag{2.27}$$

Thus the distance along the 180° focal plane between adjacent isotopes will increase directly with the radius of curvature, and it will be inversely proportional to the mass number. Hence analyzers with small radii of curvature and having a reasonable mass separation for light gases may be inadequate for the analysis of gases of high atomic mass number.

Although the 180° analyzer possesses good directional focusing properties, there are definite limitations on the sharpness of the line image, even if the ions are monoenergetic and the magnetic field is perfectly homogeneous Consider Figure 2 4, in which ions leaving a source have a half-angle of divergence, α, and rays are drawn with equal radii from centers of circular orbits from points O, O', and O". When α is large, the central ray will not coincide with the peripheral rays, and at the 180° boundary the image width will be of magnitude $\alpha^2 r$. (At the 360° boundary, i.e., initial source position, this aberration will vanish, but so will all mass dispersion).

It is obvious that the greatest resolution of ions is obtained by using a deflection of 180°. However this requires a relatively large system and a magnet of large-pole-piece area since the field must be uniform over the whole ion path. More compact and lighter mass spectrometers with deflections of 120°, 90°, and

60° were built, but the resolution of these instruments is not so high as for those with 180° angular deflection.

Besides the single magnetic deflection type mentioned above there are other types of mass spectrometers: double-focusing spectrometer, multiple magnet system, the cycloidal spectrometer, cyclotron resonance spectrometer, the time-of-flight spectrometer, quadrupole spectrometer and special type spectrometers [3].

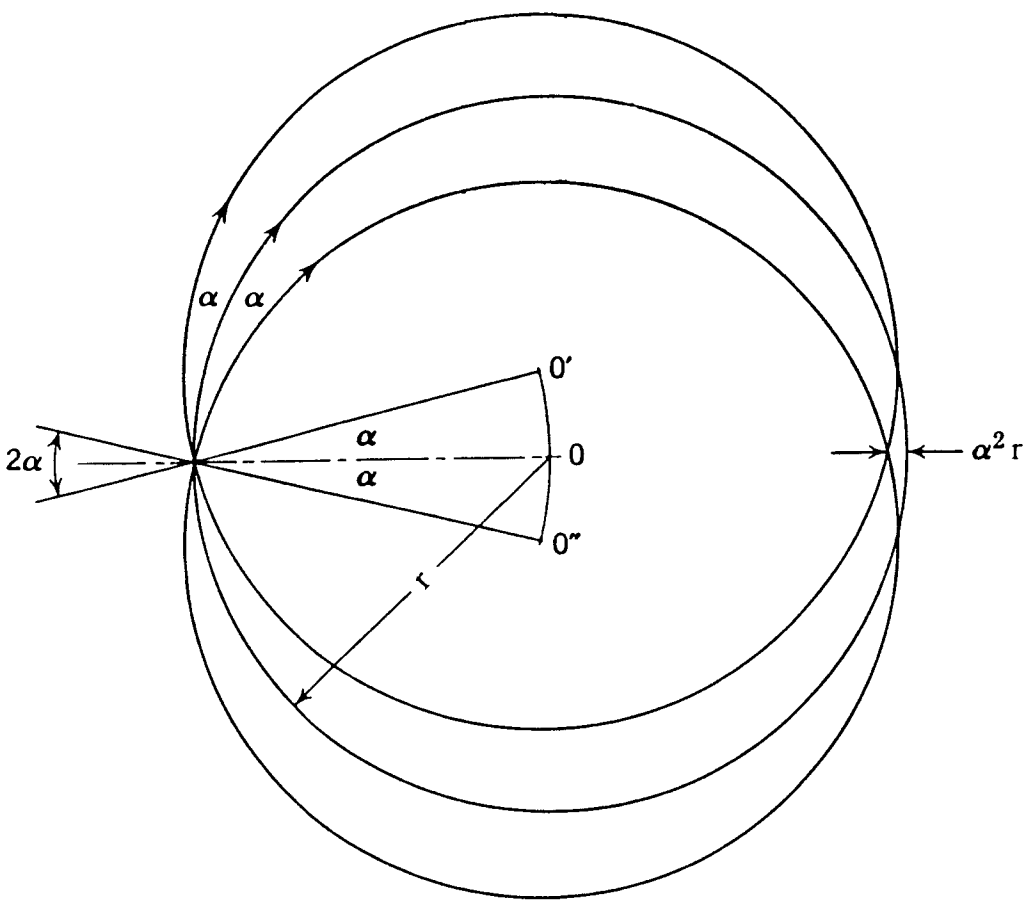

Figure 2.4 Angular aberration in the 180° sector.

2.3 Ionization Source

Ions are created in mass spectrometers by impact ionization. Figure 2.5 is an ionization chamber that might be used in a mass spectrometer. Electrons from the filament or field emitter are drawn across the chamber to the anode. While crossing this space some of the electrons collide with gas molecules, strip off one or more of their electrons, and create positive ions.

The positive ion production is not the same for all gases. Table 2.2 gives the total positive ion cross sections relative to N_2 for several common gases at an ionizing energy of 70eV. Although the ionization cross section does not peak at the same energy for all gases, it is generally greatest for most gases somewhere in the 50-to-150-eV range. The devices designed in this thesis operate at a potential between 50V and 100V and take advantage of the higher ion yield

The ion production of each species is proportional to its density or partial pressure. Consider a sample of a gas mixture containing only equal portions of nitrogen, oxygen and hydrogen whose total pressure is 3×10^{-7} Torr. A mass scan of this mixture would show three main peaks of unequal amplitudes. All other factors being equal, the main oxygen peak would be slightly larger and the hydrogen peak about half as large as the nitrogen peak because of differences in relative sensitivity or ionizer yield. If, however, the total pressure of the gas mixture were increased to 6×10^{-7} Torr, the amplitudes of each of the three main peaks would double. In other words, the instrument is linear with pressure. Linearity of the ionizer extends to a maximum total pressure of order 10^{-5} Torr. At higher pressure, space charge effects and gas collisions become important. The ions produced in the space between the filament (or field emitter) and anode are drawn out of that region, focused, and accelerated toward the mass separation space in any mass spectrometer.

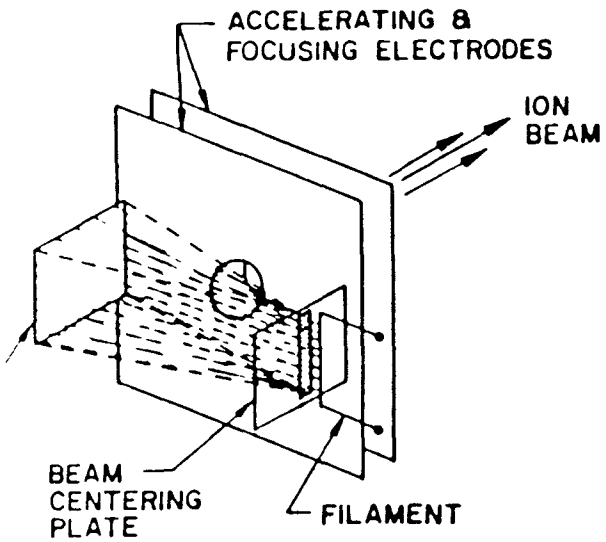

Figure 2.5 One form of an ionizing source used in a mass spectrometer [1].

Table 2.2 Experimental total ionization cross sections (70V) for selected gases normalized to nitrogen [1].

Gas	Relative Cross Section
H_2	0.42
He	0.14
CH_4	1.57
Ne	0.22
N_2	1.00
CO	1.07
C_2H_4	2.44
NO	1.25
O_2	1.02
Ar	1.19
CO_2	1.36
N_2O	1.48
Kr	1.81
Xe	2.20
SF_6	2.42

CHAPTER THREE
MICROENGINEERED MASS SPECTROMETER DEVICE CONCEPT

3.1 Background

There exists a need for a microengineered mass spectrometer. The purpose of this thesis is to scale down the dimensions of a mass spectrometer and made it portable. Simulations have shown that this device could incorporate a lateral geometry which makes its design compatible with current silicon processing technology. Uses of this device include millimeter-dimensioned ion detectors in vacuum systems, and hand-held gas detector sensors. The fabrication is also inexpensive.

3.2 Description of the Device

This mass spectrometer device uses planar geometry. It is to be fabricated on two silicon substrates approximately 1cm by 1cm, one is used as the electron source and another as the anode to collect the ions. It utilizes an electrostatic and a magnetic field to have the ions with different masses separated and collected by adjacent and coplanar anodes. A 3000 Gauss magnetic field permits collection of ions of up to approximately 222amu (radon) for the special dimensions used. Power supply voltage levels are 0 and V_a For static magnetic fields of 3000 Gauss, the required value for V_a is 50V. Schematic diagrams of this device are shown in Figure 3.1. Chip A is approximately 1cm by 1cm. There is a strip of tip arrays about 1cm by 0.2cm on chip A The total number of tips is about 45,000. Chip B measures 1cm by 1.5cm. There are several ion collectors on this chip. Each collector is used for a specific molecular weight of singly ionized gas ions.

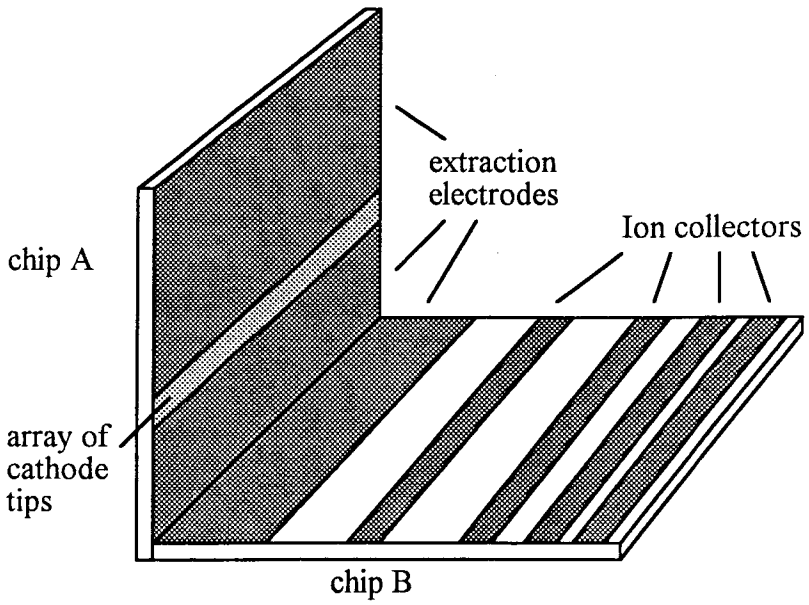

(a)

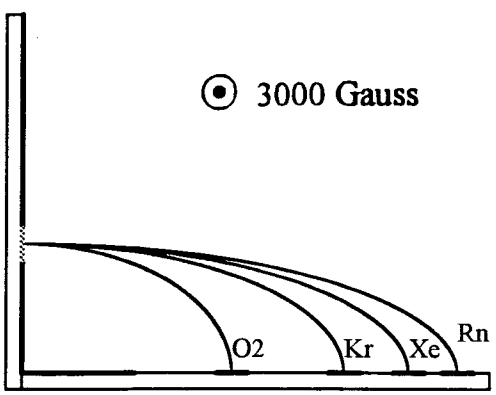

(b)

Figure 3.1 Schematic diagram of microengineered mass spectrometer: (a) isometric view; and (b) side view showing the ion trajectories.

The principle of operation is as follows: The electrons are emitted from the cathode tips and enter what will be referred to as the "active region". In the "active region", the electrons accelerated by electric field, collide with gas molecules, and cause them to be ionized. For hydrogen, for example, the ionization process for single ionization is,

$$H + e^- \rightarrow H^+ + 2e^-.$$

In order for this occur, the incident electrons must have sufficient energy to cause an electron to be released by hydrogen atom. This minimum energy is known as the ionization energy or ionization potential of the atom. For hydrogen, there is only a single electron present, and therefore no more than one can possibly be liberated. However, for atoms with more than one electron, it is possible for multiple ionization to occur. The energy required for the second ionization is in general higher than that required for the first, which means that a second ionization is less likely to occur than the first. Once ionization has occurred, the ions are accelerated by the electric field set up by the electrodes, and are caused to move in a curved trajectory by a combination of the electric field and an applied magnetic field. Finally, the separated ions are collected on the ion collectors (anode) The location of these collectors depends on the computer simulation result of ion trajectories.

As mentioned in chapter two, the mass spectrometers do not actually respond to mass, but rather to the ratio of mass to charge. For this reason, it is possible that if a given mass particle were ionized twice, it would look the same to the mass spectrometer as a singly ionized particle of half its mass. However, since the second ionization energies are higher than the first [4], this situation is much lower probability. The design of this device is such that the electrons cannot in most cases attain enough energy to cause a second ionization.

3.3 Ion Trajectory Analysis

In this chapter, several mass spectrometers devices were designed, simulated, and compared. SIMION is employed to simulate the trajectories.

SIMION is an electrostatic lens and design program [5]. In SIMION, an electrostatic lens is defined as a 2-dimensioned electrostatic potential array containing both electrode and non-electrode points. The potential array is refined using over-relaxation methods allowing voltage contours and ion trajectories to be computed and plotted. Magnetic field can also be specified for computing ion trajectories in many electrostatic and magnetic field environments.

Figure 3.2 shows the device I which uses only one substrate. This device is a surface engineered planar structure. Its length is 1.5cm, width is 1cm. Due to the relatively small size of the active region compared to the overall size of the substrate, it was necessary to simulate the active region separately from the ion collection region of the device. Figure 3.2(a) shows the entire region while Figure 3.2(b) shows the active region. The ratio of the scale of these two figures is 10:1. Electrode A is an electron collector with 50V. B and C are both focal electrodes with -20V and -50V respectively. D1, D2, D3, and D4 are all 0V. Cathode tips on the substrate are grounded Magnetic field is 3000 Gauss (with out of paper direction). Electrons are field emitted from cathode tips and collected by electrode A. Ions created in the active region are attracted by electrode B, focused by electrode C, and finally collected by one of collector D1, D2, D3, or D4.

Figure 3.3 shows the device II with two substrates. The vertical substrate (chip A) containing the cathode is 1cm by 1cm and the lateral substrate containing the anodes is 1.5cm by 1cm. Figure 3.3(a) shows the entire device II with ion trajectories. Figure 3.3(b) is expanded 10x to show the active region. The surface of the vertical substrate is biased at 50V, but the cathode tips array is grounded. Ion collectors D1, D2, D3, and D4 on the lateral substrate (chip B) are also

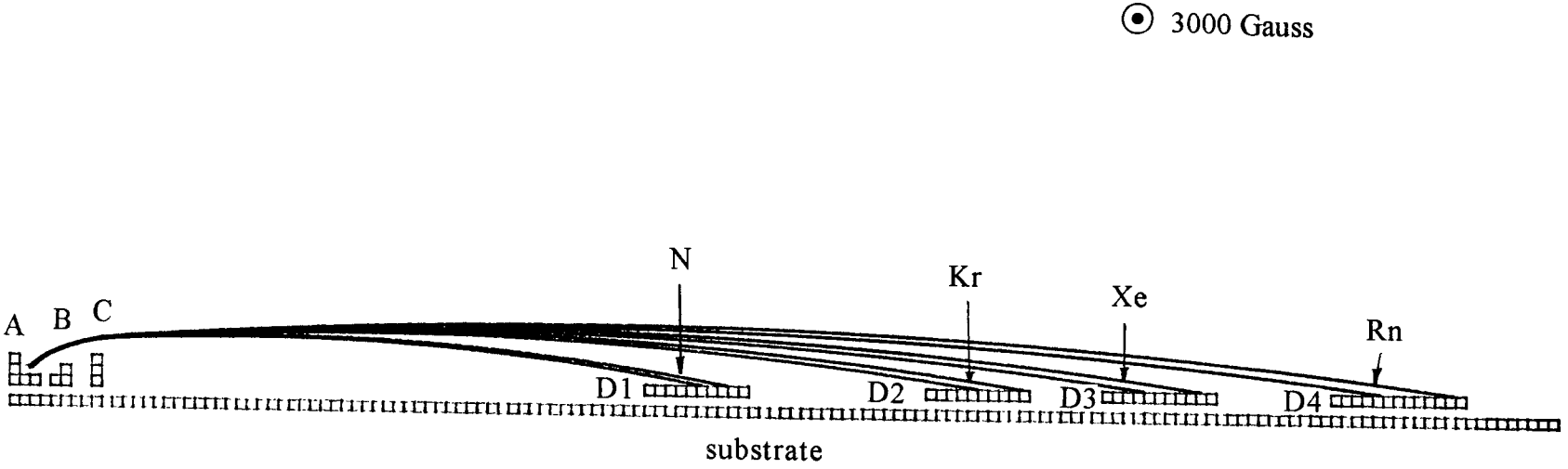

Figure 3.2(a) Planar device I showing ion trajectories for nitrogen, krypton, xenon, and radon. Magnetic field is 3000 Gauss A, B, and C electrodes are biased at 50V, -20V, and -50V respectively. D1, D2, D3, and D4 are all biased at 0V. The scale unit is 0.1mm per square.

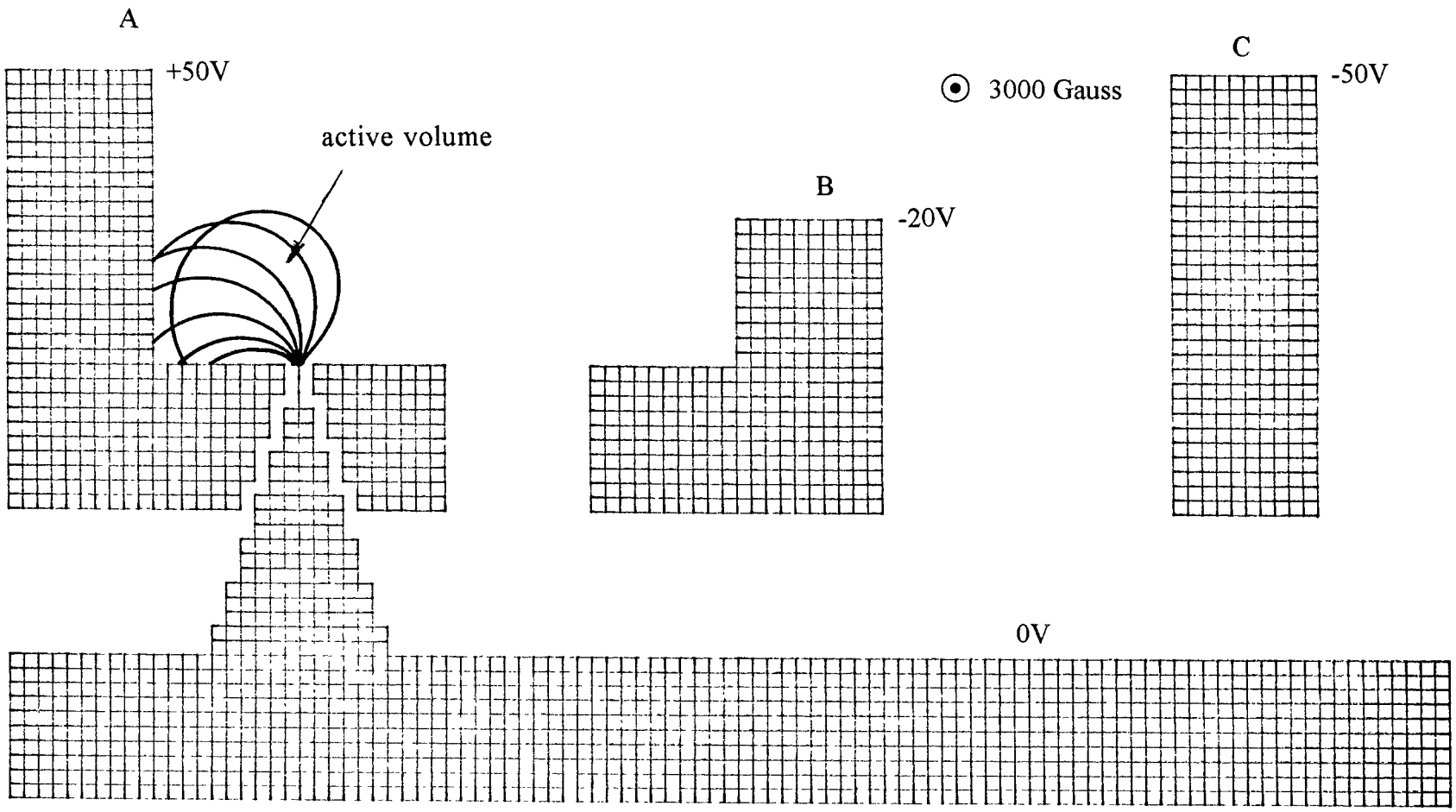

Figure 3.2(b) Close in electron cathode region of device I with cathode tip showing trajectories of electrons and ions. The scale unit is 0.01mm per square.

maintained at near ground potential. The main advantage of device II is that the sensitivity was greatly increased due to its larger active region (between the initial point of the highest and lowest ion trajectories in figure 3 3(a)).

The sensitivity results from the ions created and detected (collected). An increased volume of the ionizing active region results in additional ionization and a resulting higher sensitivity. The ionizing active region is very close to the cathode tips The ionizing volume is determined by the total number of tips However, as the volume of the active region is increased beyond certain special limits, overlap of ion trajectories will occur. This means ions with different mass, for example, Xe^+ and Rn^+ can not be separated and collected by adjacent collectors D3 and D4 respectively. A portion of Xe^+ will be unacceptably collected on radon collector D4 and a portion of Rn^+ will also be unacceptably collected on xenon collector D3. Figure 3.4 shows the simulation of the trajectory overlap problem. Trajectories of Xe^+ Rn^+ are selected for illustration in this figure. Overlap will reduce resolution of this device. The trade-off should be made between sensitivity and resolution. Detailed calculation of sensitivity will be discussed in chapter four. Since many factors, for example, the uniformity of applied magnetic field, the sharpness of tips, the distance between neighboring tips, will effect a change in resolution, the calculation of resolution is very complicated. The computer simulation results provide trajectory information in which the magnetic field is assumed to be uniform. Trajectories for different gas species which do not overlap in the SIMION simulation plot are indicative of the desired performance.

After many simulations, it was found that if an electrode was added to the left side of chip B (figure 3.3(a)) with the same voltage as that on the surface of chip A (50V), the active region could be larger but without ion trajectories

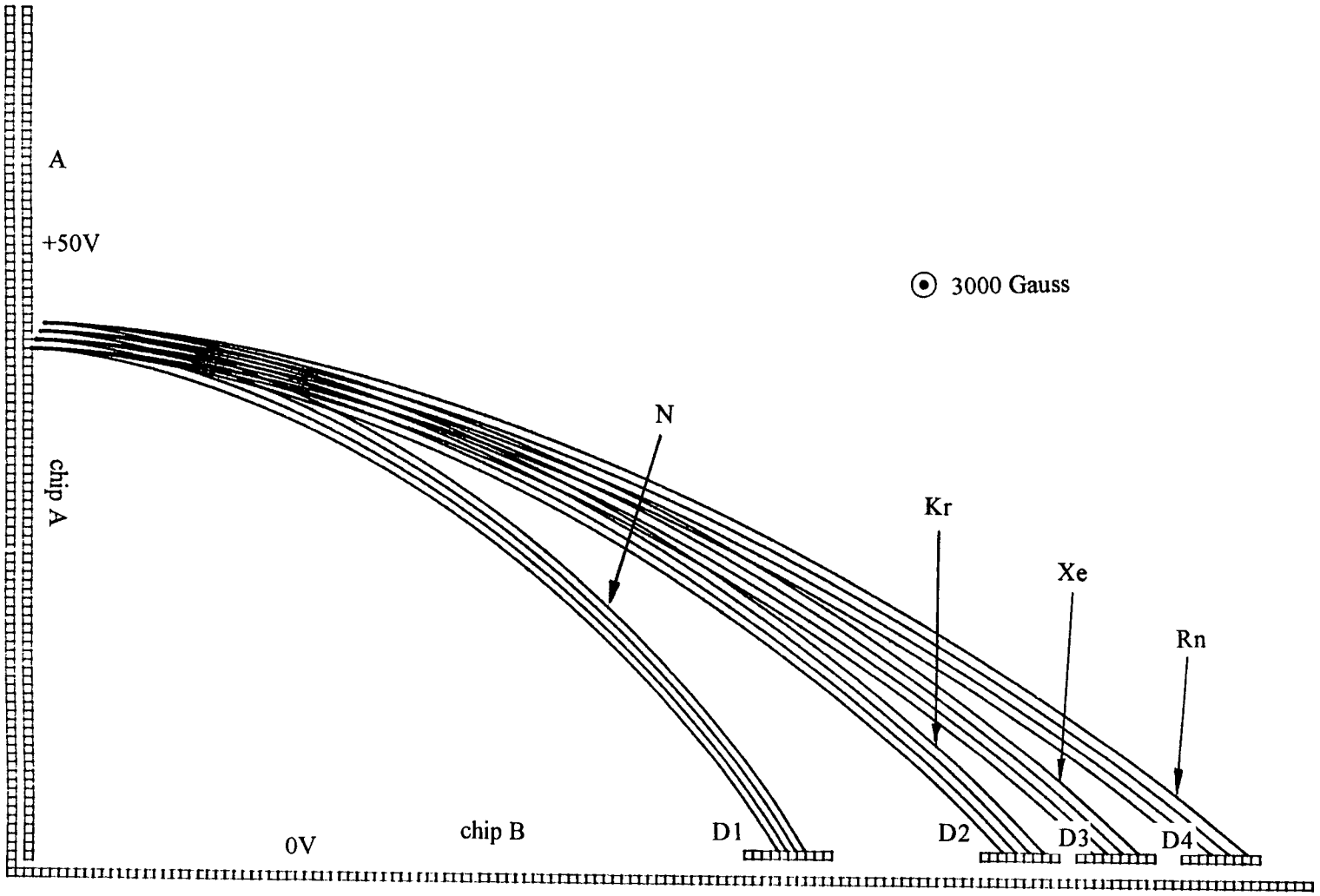

Figure 3.3(a) Device II showing ion trajectories for nitrogen, krypton, xenon, and radon. Magnetic field is 3000 Gauss. A is biased at 50V. D1, D2, D3, and D4 are maintained at near 0V. Substrates are grounded. The scale unit is 0.1mm per square.

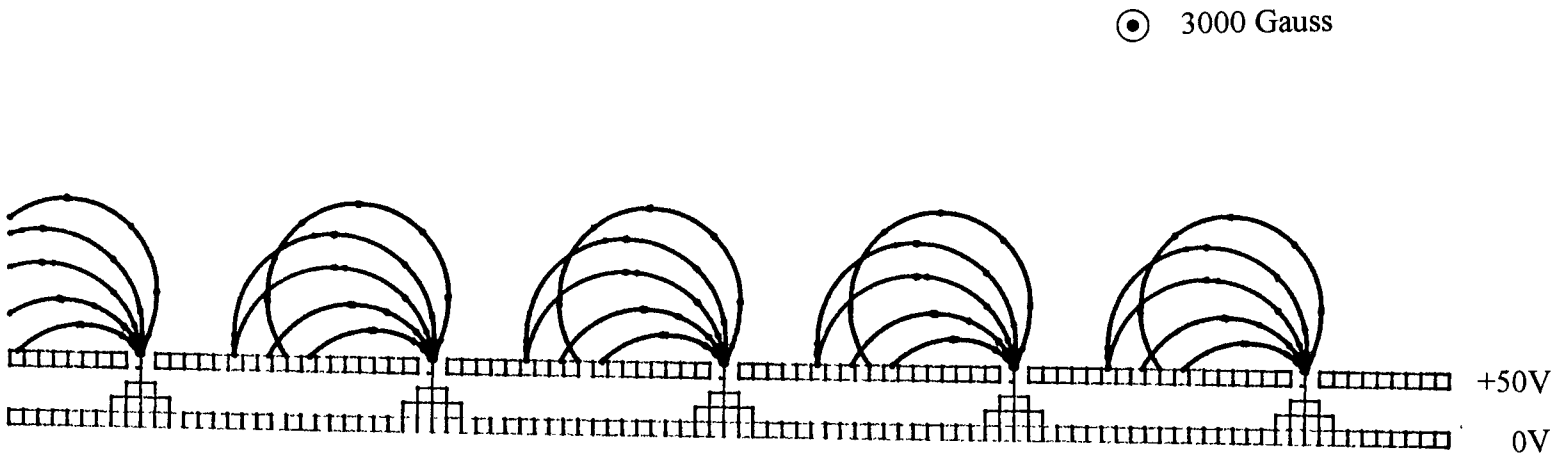

Figure 3.3(b) Close in electron active region of device II with cathode tip array showing electron trajectories. The scale unit is 0 01mm per square.

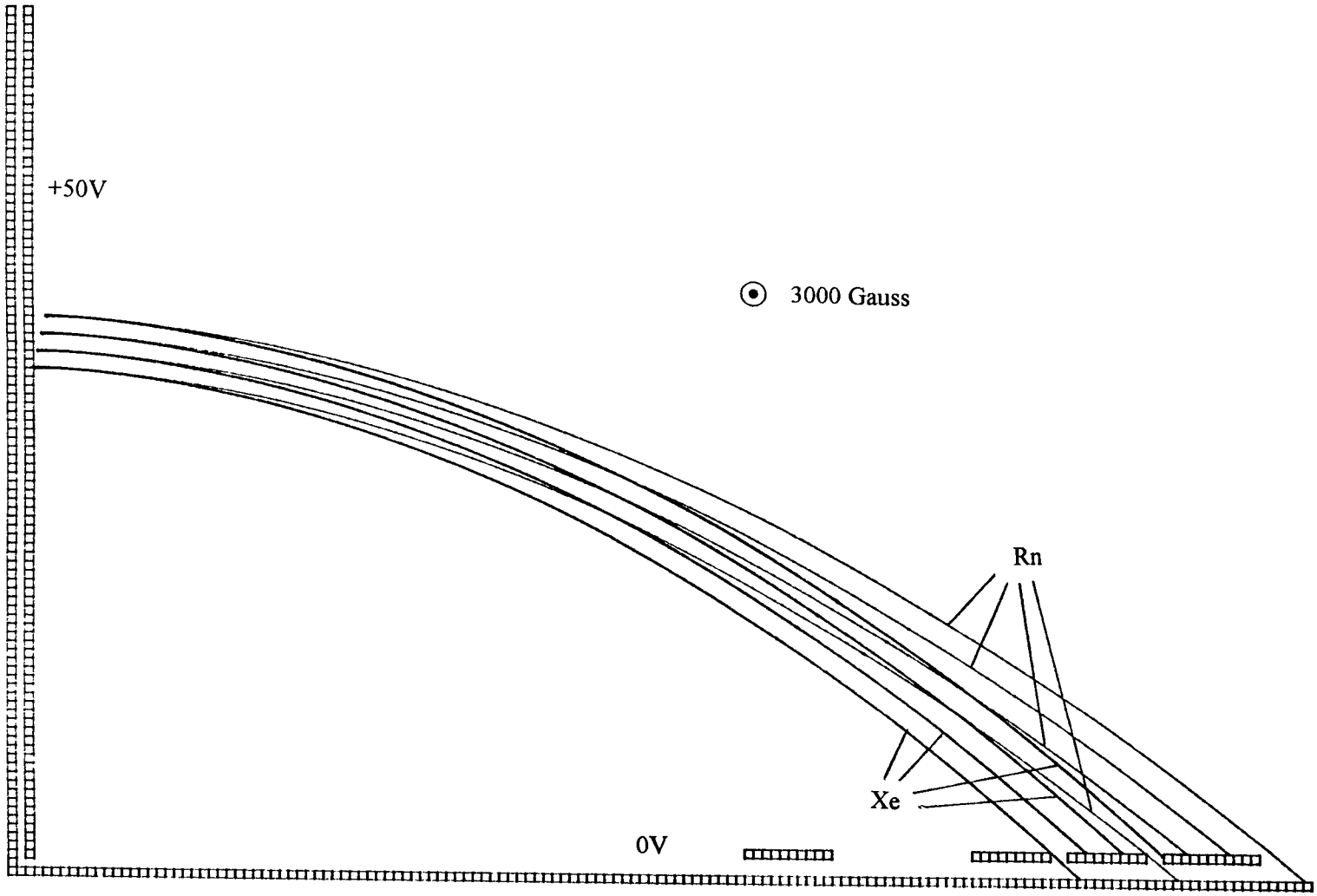

Figure 3.4 Xenon and Radon ion trajectories overlap. Ion collectors are maintained at near 0V. The scale unit is 0.1mm per square

overlap. Figure 3.5 shows the device III. The added electrode F acts like a focal electrode. The ion separation is much better than device II.

This microengineered mass spectrometer can be configured as a the time-of-flight mass spectrometer. Simulation results shows that the average flight times (from the ionizing event to ion collection) for nitrogen, krypton, xenon, and radon are 1.2μs, 2,2μs, 2.9μs, and 4.1μs respectively. These time intervals are large enough for sensing.

3.4 Summary

By comparing device I design, device II design, device III design, and many other structures which are not shown in this thesis, the optimized geometry of the microengineered mass spectrometer was determined to be device III. It can be seen from figure 3.5 that nitrogen, krypton, xenon and radon ions are adequately separated by device III. The active region of device III is the largest. It provides maximum sensitivity. The remainder of this thesis describes device III.

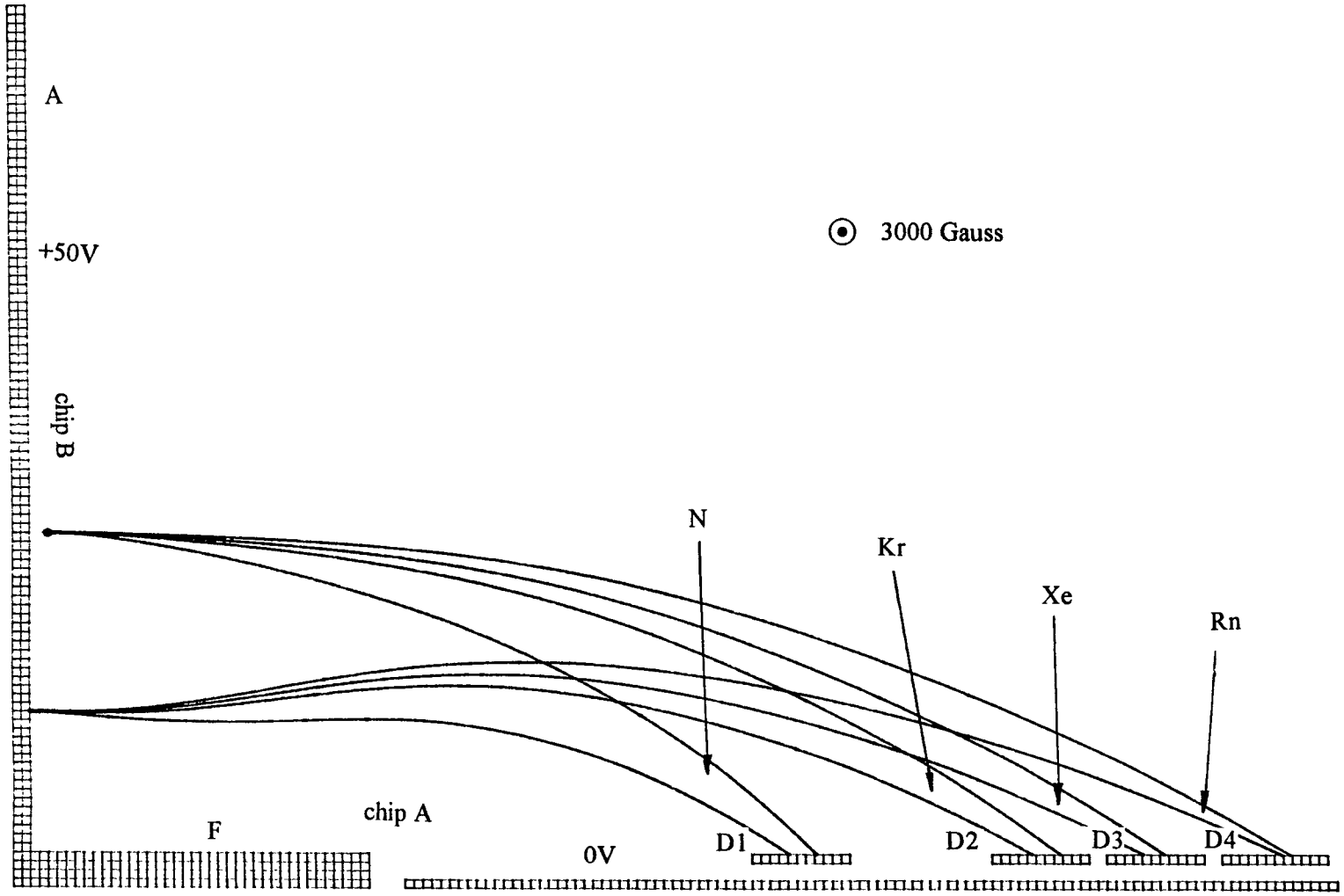

Figure 3.5 Device III showing ion trajectories for nitrogen, krypton, xenon, and radon. Magnetic field is 3000 Gauss. A, and F are connected and biased at 50V. D1, D2, D3, and D4 are maintained at near 0V. Substrates are grounded. The scale unit is 0.1mm per square.

CHAPTER FOUR
CATHODE DESIGN

The critical electrodes in the microengineered mass spectrometers are the cathode tips. The location of the cathode determines the active, ionizing region. The electrons emitted from tips must ionize molecules in and only in the active region. Any ionization activity outside the active region will generally cause dispersion Other important parameters in the cathode design are the electron current density emitted from cathode tips, and the electron trajectories. They are decided by applied electric and magnetic fields, tip sharpness and distance between individual tip and gate (electron extraction electrode). This chapter presents the design for cathodes.

4.1 Electron Trajectory Analysis

Figure 4.1 shows the near-field trajectories of electrons emitted from the cathode tip array In the design, trial values for the voltage of electrodes and the magnetic field were selected Then ion trajectories were simulated by the aid of the SIMION program. Basically, the design requires that the maximum volume for the active, ionizing region be selected which will permit isotope separation. This is done by changing the starting point coordinates of ions ($x \rightarrow x+\Delta x$, $y \rightarrow y+\Delta y$) until the overlap of some ions with different mass occurs. See the optimized design shown in Figure 3.5 in chapter three, the changes of ion staring point coordinates Δx and Δy are 0.2mm and 2mm respectively. The product of $w \times \Delta x \times \Delta y$ is defined as the volume of active region, where w is the width of the substrate (w=1cm in this design). The location of the cathode tips array must be within the area $w \times \Delta y$ so that all emitted electrons can only travel in the active region. Figure 4.2 shows a view of the cathode-tip array (chip A) and the active region (enclosed by dotted lines).

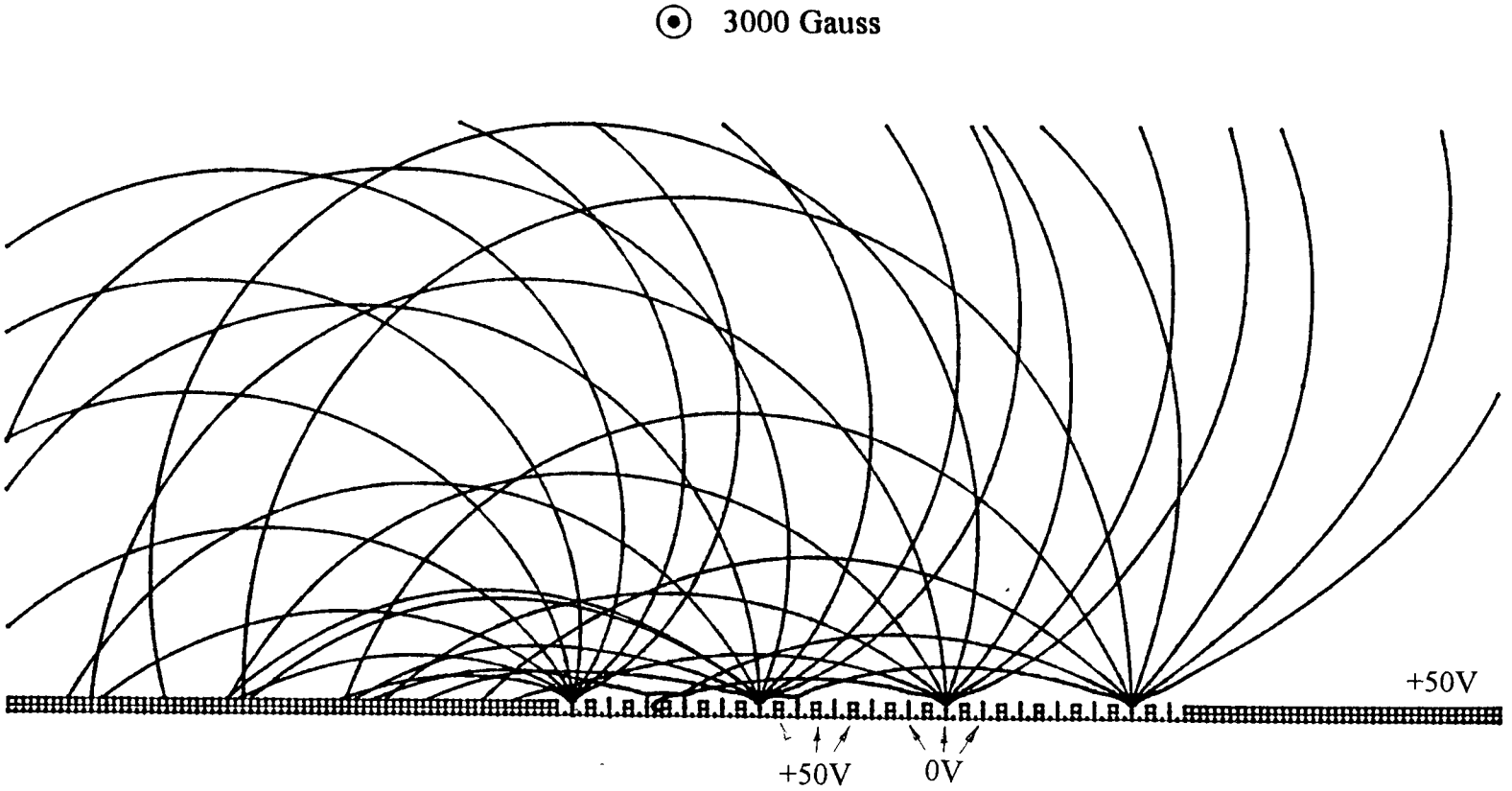

Figure 4 1(a) Trajectories of field emitted electrons. The scale unit is 5μm per square

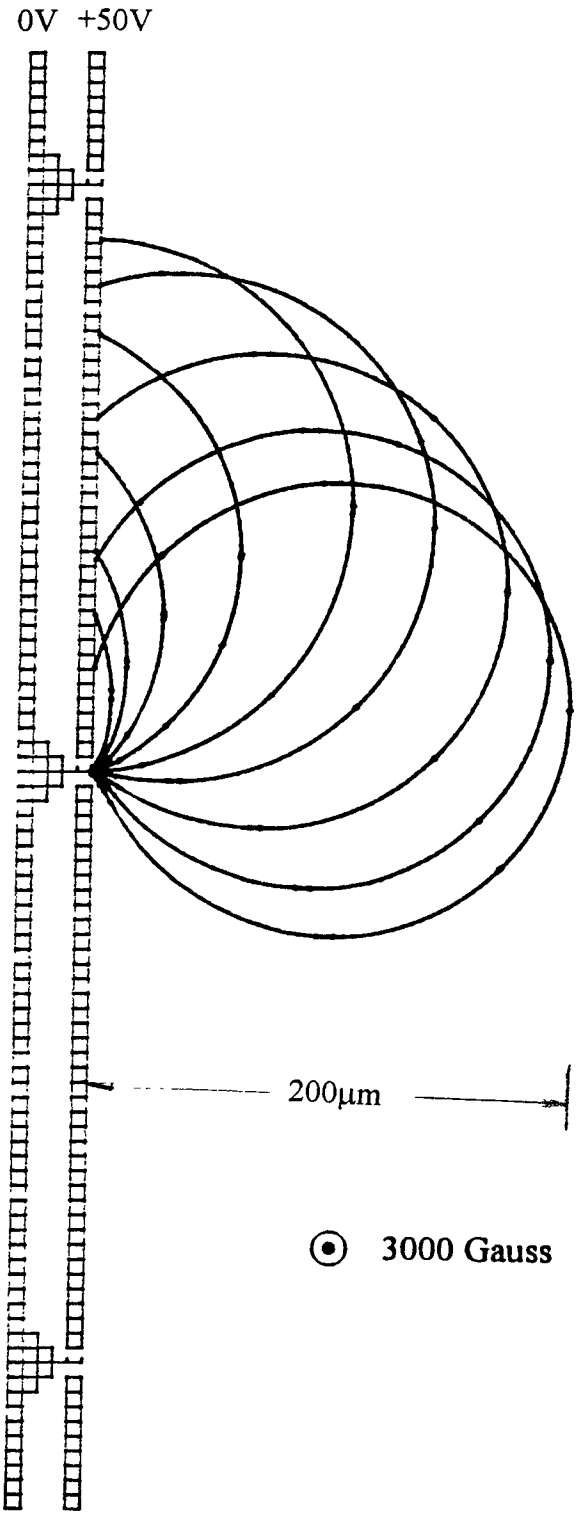

Figure 4.1(b) Electrons emitted from one of the tips. The scale unit is 5μm per square.

Simulation result also shows that the electron trajectories of most electrons are approximately a semicircle (Figure 4.1(b)). The maximum height of trajectories is less than 200μ. Since no electron is beyond this height, there are no ions created. Therefore the design requirement $\Delta y \leq 0.2$mm is satisfied.

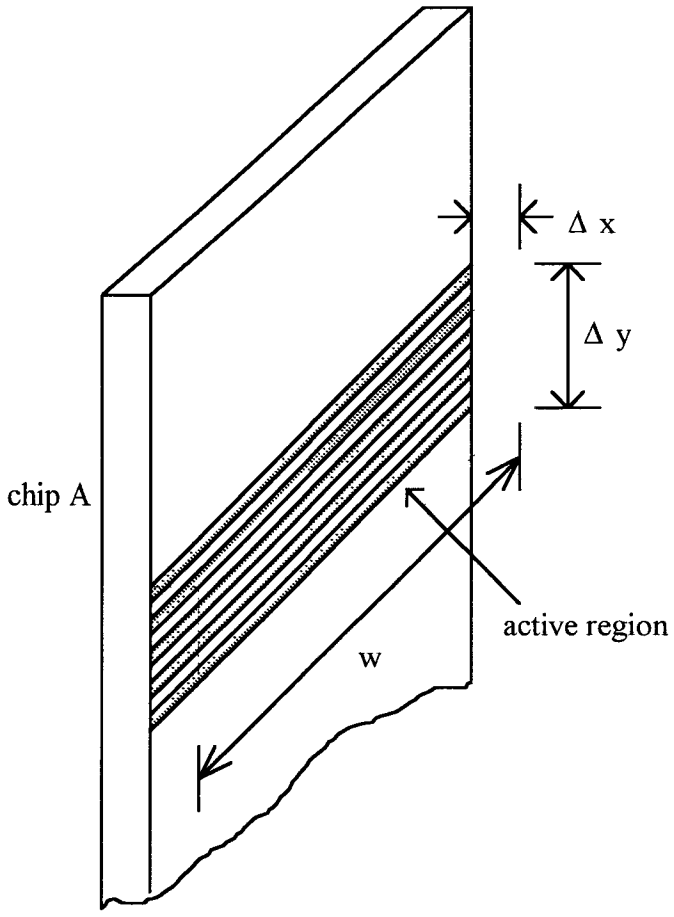

Figure 4.2 A portion of chip A showing the active region (enclosed by dotted lines).

Due to the very small size of active region compared to the overall device dimensions, it is impossible to observe electron paths at the cathode tips when simulating ion trajectories. The limited resolution for the SIMION simulation does not permit simultaneous plots of electron and ion trajectories within the same field. Zooming techniques are available but are not used in this design. The maximum matrix size for SIMION version 4.0 is 16,000 array points. In the ion trajectory simulation the tips array was simply treated as a conducting plane of 50V potential (refer to Figure 3.5, electrode A). In the real device, the tip inside the small gate opening is grounded and will modify the electrostatic field and hence the ion trajectory slightly. The contour of the electrostatic field near a gate opening is shown in Figure 4.3. Ions created near the gate opening might be dispersed caused by the curvature of electric contours (Figure 4.3(a)). To reduce ion dispersion, the cathode tips array were divided into ten smaller arrays. Each smaller array contained three lines of tips. The distance between adjacent smaller arrays is about 200μ. This is larger than the diameter of the trajectory of most electrons. Because there are no gate openings within the 200μ-region where ions are created, the electric field is uniform and overall ion dispersion is reduced (Figure (4.3(b)). In the region very near the tip, electrons do not yet have enough kinetic energy to strip off an electron from a molecule (ionize) upon impact. This cathode design reduces the dispersion of ions at the ion collector.

The cathode used in the device III is a lateral geometry. It has simple structure compared to vertical geometry But the current density of the lateral geometry is lower than that of the vertical geometry. Since there are a large number of tips on the cathode of device III (total number of tips is 37.5k). This provides enough electron cathode current for ionization.

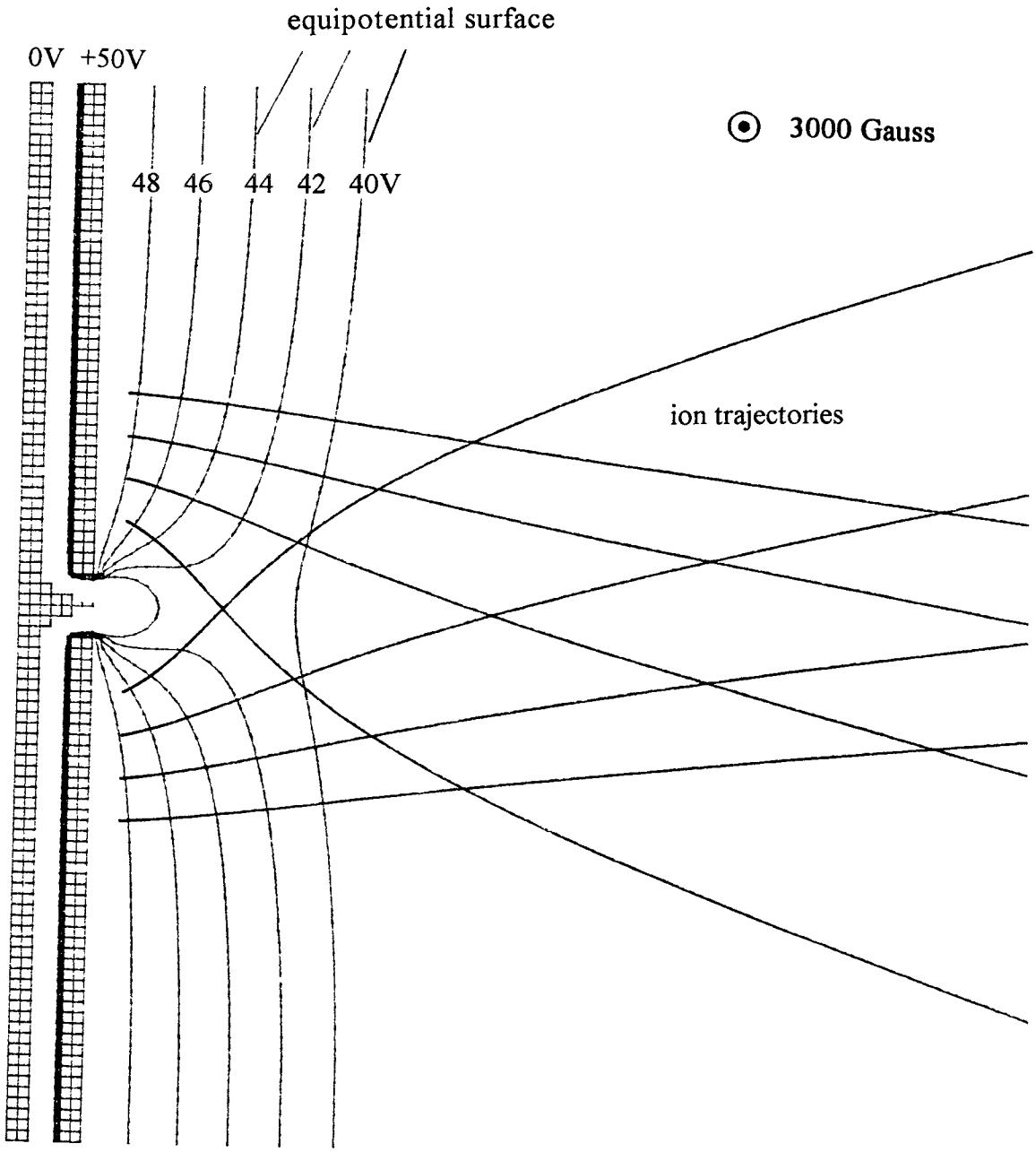

Figure 4.3(a) Illustration of dispersed ions trajectories. Ions originating near the cathode have higher dispersion. The scale unit is 1μm per square.

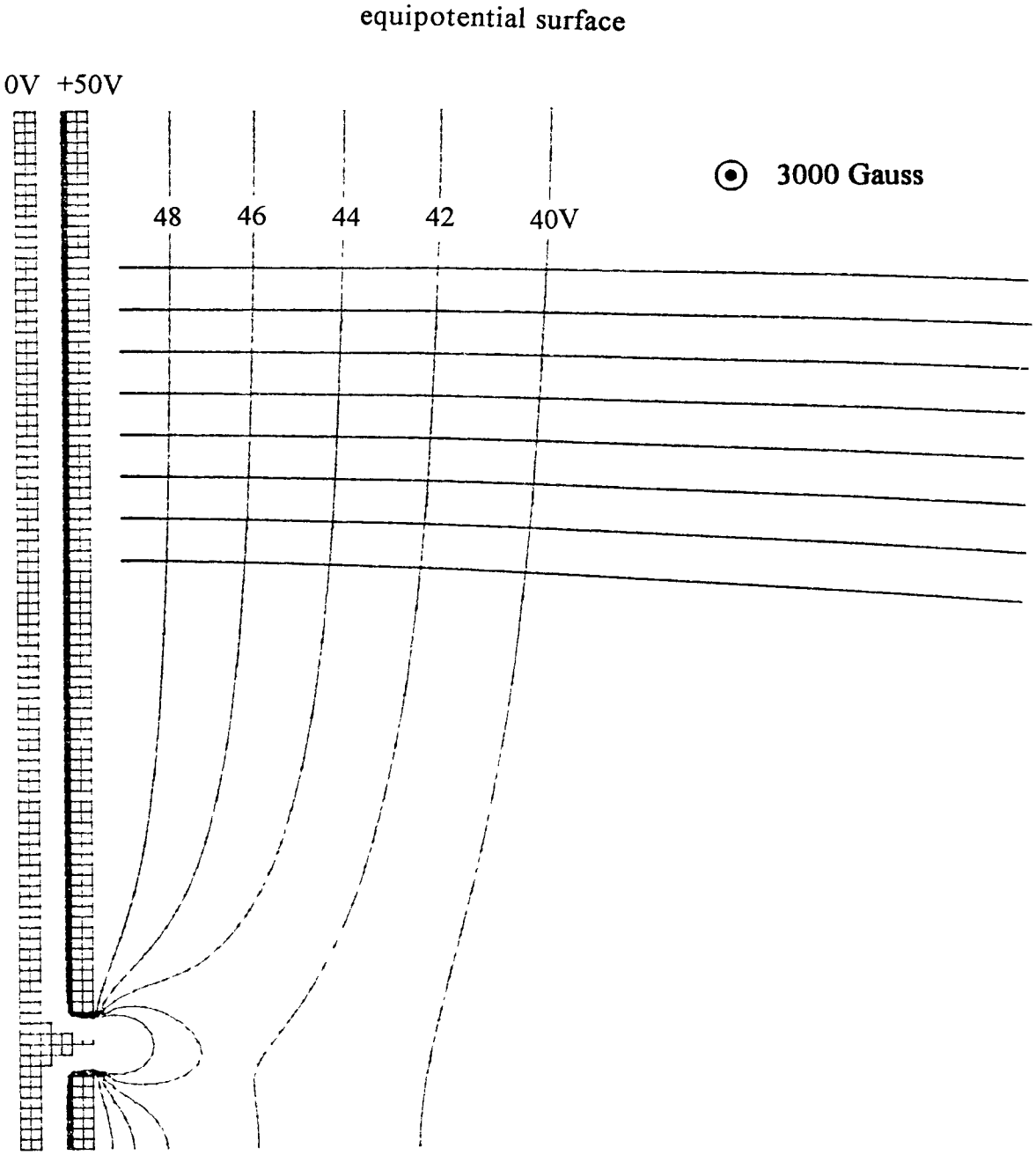

Figure 4.3(b) Selected ion trajectories (m=222) illustrating minimal local dispersion effect due to proximity to high E-field. Ions originating far from the cathode tip have no dispersion. The scale unit is 1μm per square.

4.2 Sensitivity Parameter modeling

A very important parameter in designing the microengineered mass spectrometers is the sensitivity. A very high sensitivity is required to detect trace gases such as radon. This sensitivity is defined as [6] the quotient of the ion current at the collector and the partial pressure of the gas present in the ion source. The calculation is based upon molecular ionization theory.

When an electron is moving with a velocity v and then collides with an atom, kinetic energy is exchanged. If no excitation or ionization results, such a collision is an elastic collision. The collision becomes inelastic if the gas atom or molecule is excited or ionized by acquired energy from the incident electron Since there are a large number of particles in a gas and the characteristics of their paths cannot be determined, the collision frequency cannot be calculated or measured at any given instant. However, because of the very large number of molecules present, it can be assumed that when the system is in equilibrium, they are uniformly distributed in space, and their velocities are distributed according to the Maxwell-Boltzmann law. Under these conditions, the fluctuations in the frequency of collisions about a mean value are very small. When an electron is injected into the gas with a velocity v, the probability of a collision of a given type occurring is

$$d\varpi = n\sigma \cdot dl \tag{4.1}$$

where n is the number of particles per unit volume of gas, σ is the cross section of the collision, and dl is the distance traveled in the gas. The mean free path λ is the reciprocal of the total cross section $n\sigma$

$$\lambda = \frac{1}{n\sigma}. \tag{4 2}$$

If an electron beam flux rate N (electrons/sec) is introduced into the gas, then the average number of collisions dN in a distance dx will be approximately

$$dN = N \cdot d\varpi = Nn\sigma \cdot dx \tag{4.3}$$

The concept of collision cross section can be made useful in describing the impact process and its products. If the electrons undergo $n\sigma$ collisions per unit path, some collisions will be elastic, and another portion will be inelastic which will ionize or excite the molecules impacted. The total number of collisions per unit length is [7]

$$\frac{dN}{dx} = Nn\sigma = Nn(\sigma_{el} + \sigma_{ion} + \sigma_{ex}) \tag{4 4}$$

where σ_{el}, σ_{ion}, and σ_{ex} are cross section for elastic, ionizing, exciting collisions respectively. The number of ionizing collisions per unit length is

$$\frac{dN_{ion}}{dx} = Nn\sigma_{ion}. \tag{4.5}$$

The fraction of collision events that are ionizing f_{ion} is obtained by dividing the number of ionizing collisions $n\sigma_{ion}$ by the total number of collisions $n\sigma$. Thus

$$f_{ion} = \frac{n\sigma_{ion}}{n\sigma} = \frac{\sigma_{ion}}{\sigma} = \frac{\lambda}{\lambda_{ion}} \tag{4.6}$$

where $\sigma=\sigma_{el}+\sigma_{ion}+\sigma_{ex}$.

The values of the ionization cross section σ_{ion} for the rare gases, resulting from collision with electrons of energies between 10eV and 100eV are given in Figure 4.4 where a_0 is about 0.05nm. The ionization cross sections are energy dependent and the maximum values occur between 80eV and 200eV, above which the cross section decreases quite rapidly. The increase in cross section is much more rapid between 10eV and 25eV. These curves show that cross sections increase as the atomic size of the atom increases. The ionization cross section σ_{ion} for the common gases N_2, O_2, and H_2, is given in Figure 4.5 for comparison These curves exhibit exactly the same features as those of the rare gases

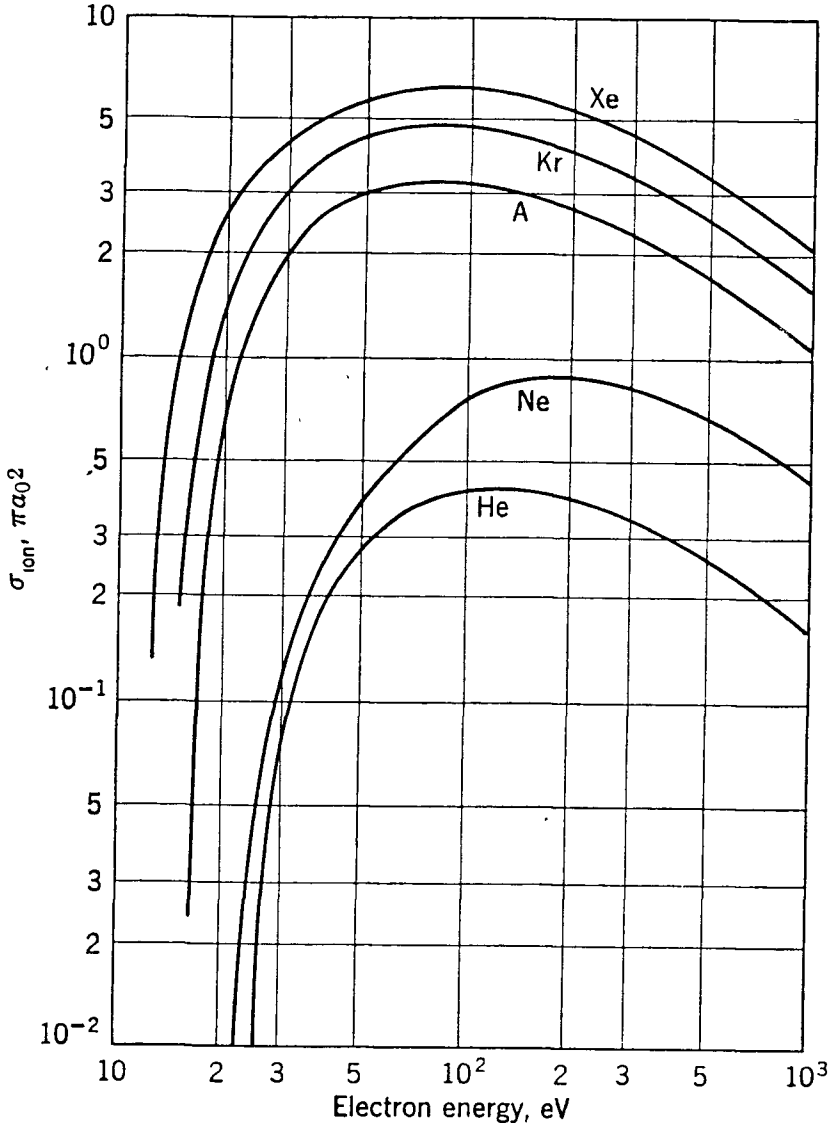

Figure 4.4 Ionization cross section σ_{ion} for the rare gases due to electron impact given in units of πa_0^2, where $\pi a_0^2 = 8.82 \times 10^{-17} cm^2$, a is the radius of H-atom in ground state $a \approx 0.05nm$ [7].

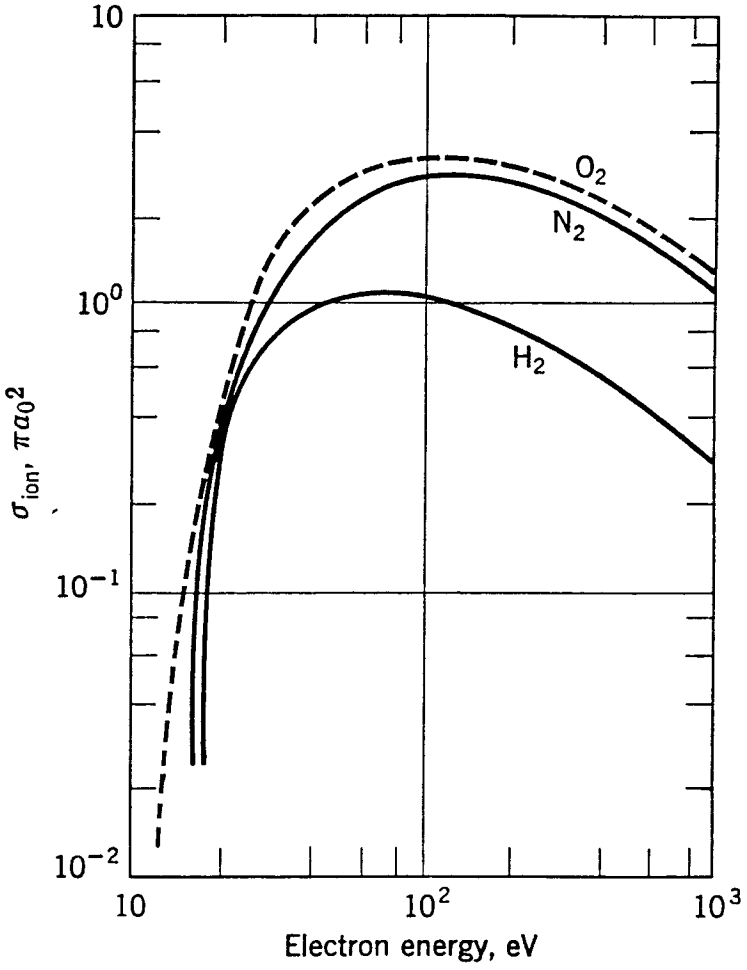

Figure 4.5 Ionization cross section σ_{ion} for O_2, N_2, and H_2 due to electron impact given in units of πa_0^2 [7].

The sensitivity of the microengineered mass spectrometer can be calculated by using the discussed ionization cross section. The beam of N electrons per second emitted from the array of cathode tips traveled through the active region in a semicircle trajectory (Figure 4.1(b)). The average diameter of the semicircle is 160μ (max. 200μ). The average distance that each electron travels to the anode is

$$l = \pi \cdot r = \pi \cdot 80\mu m \approx 251\mu m \tag{4.7}$$

The average number of ionizing collisions Ω between electrons and molecules per second is

$$\Omega = Nn\sigma_{ion}l \tag{4.8}$$

where n is the density of gas molecules and N is electron flux rate (total number of electrons/sec emitted from the cathode). Assuming all ions are collected by the ion collector, then the total ion current I_+ is

$$I_+ = Nen\sigma_{ion}l \tag{4.9}$$

where e is the charge of the electron. Since N·e is the total cathode current I_-, equation (4.9) becomes

$$I_+ = nI_-\sigma_{ion}l. \tag{4.10}$$

The ion current I_+ can be related to the partial pressure P of the gas species using equation (2.4) to substitute n The ion current I_+ becomes

$$I_+ = 9.656 \times 10^{18} \frac{P}{T} I_-\sigma_{ion}l \tag{4.11}$$

where P is expressed in Torr, T is in absolute temperature °K, σ_{ion} is in cm^2, and l is in cm.

Conversely, if I_{+min} is the minimum detectable current for the ion collector, then the minimum detectable pressure P_{min} becomes

$$P_{min} = 1.0356 \times 10^{-19} \frac{I_{+min}T}{I_-\sigma_{ion}l}. \tag{4 12}$$

Using the above equations, we can now estimate specific performance parameters for the microengineered mass spectrometer. For example, if the minimum detectable ion current I_{+min} is 10fA, the electron current I_{t-} emitted from each tip is 0.1μA, the total number of tips j is 37500, then the total cathodes current is

$$I_- = jI_{t-} = 37500 \times 0.1\mu A = 3.75mA \qquad (4\ 13)$$

From Figure 4.4 we can obtain the ionization cross section of xenon at electron energy of 30eV

$$[\sigma_{ion}]_{Xe} \approx 4\pi a_0^2 = 4 \times 8.82 \times 10^{-17} cm^2 = 3.53 \times 10^{-16} cm^2. \qquad (4.14)$$

From equations (4.13), (4.14) the minimum detectable xenon partial pressure P_{minXe} at temperature of 25°C is

$$P_{minXe} = \frac{1.0356 \times 10^{-19} \times 10^{-14} \times 298}{3.75 \times 10^{-3} \times 3.53 \times 10^{-16} \times 0.0251} \approx 9.3 \times 10^{-12} (Torr) \qquad (4.15)$$

This important parameter is the detection limit for this device sensing xenon in a very high vacuum range. Equation (4.15) assuming that 100% of the ions are collected to the ion collector electrode. If only 10% of the ions are collected, for instance, this device can still measure a minimum xenon partial pressure of 10^{-10} Torr at room temperature.

Since the mass of radon (222amu) is greater than that of xenon (131amu), the ionization cross section of radon is also larger than that of xenon. Thus minimum detectable pressure of radon is lower than that of xenon for this device. Figure 4.6 is the plot of detectable gas partial pressure vs. minimum detectable ion current for He, Kr, Xe, and Rn based on equation (4.12).

Another important performance parameter is the ionization efficiency η_{ion} in the region of the cathode. It is defined as the ratio of the average number of ions created in the active ionizing volume per second I_+/e to the total number of molecules entering this volume per second Φ

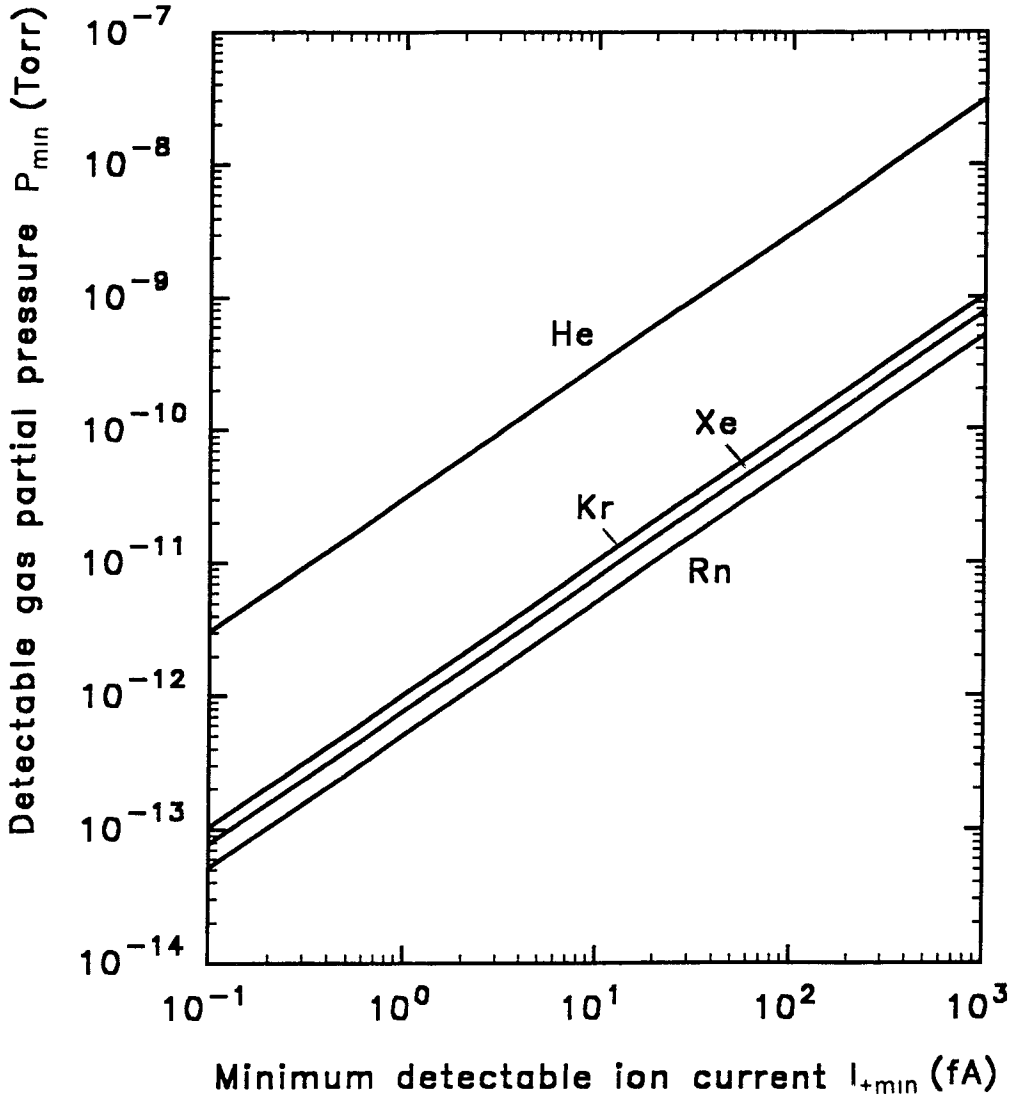

Figure 4.6 Detectable gas partial pressure vs minimum detectable ion current for He, Kr, Xe, and Rn.

$$\eta_{ion} = \frac{I_+}{e\Phi} \tag{4.16}$$

where e is an electron charge (1.6×10^{-19} Coul). In Figure 4.2, the surface area (enclosed by dotted lines) is

$$S = 2(\Delta x \cdot \Delta y + \Delta x \cdot w) + \Delta y \cdot w. \tag{4.17}$$

For the specific ionizing volume surrounding the cathode in this device, Δx is 0 2mm, Δy is 2mm, and w is 10mm. Thus

$$S = 2 \times (0.2 \times 2 + 0.2 \times 10) + 2 \times 10 = 24.8(mm^2) = 0\ 248(cm^2). \tag{4 18}$$

From equation (2.10), the molecular flux rate Φ becomes

$$\Phi = \phi S = 3.513 \times 10^{22} \cdot \frac{PS}{(mT)^{1/2}} \tag{4.19}$$

where P is in Torr, m is the gas molecular weight, S is in cm^2, and T is the absolute temperature. Substituting equations (4.11), (4.18), and (4.19) into (4.16), one obtains

$$\eta_{ion} = \frac{9.656 \times 10^{18} \frac{P}{T} \cdot \frac{I_-}{e} \cdot \sigma_{ion} \cdot l}{3.513 \times 10^{22} \frac{PS}{(mT)^{1/2}}} = 2\ 75 \times 10^{-4} \left(\frac{m}{T}\right)^{1/2} \frac{I_- \sigma_{ion} l}{eS} \tag{4.20}$$

where I_- is the total cathode current, e is electron charge, and l is the average distance that each electron travels (in cm). For this device, I_- is 3.75mA (equation (4.13)), l is 0.0251cm (equation (4.7)), and S is 0 248cm^2. If the gas is xenon, for example, m is 131amu, σ_{ion} is $3.53\times10^{-16}cm^2$, environment temperature is 25°C, then the efficiency η_{ion} becomes

$$\eta_{ion} = 2.75 \times 10^{-4} \left(\frac{131}{298}\right)^{1/2} \frac{3.75 \times 10^{-3} \times 3.53 \times 10^{-16} \times 0.0251}{1.6 \times 10^{-19} \times 0.248} \approx 1.53 \times 10^{-4} \tag{4.21}$$

This efficiency is a small value and is due to the small cathode current. It can be concluded that cathode electron current determines the ionization efficiency. The

minimum detectable partial pressure P_{min} can be reduced significantly by increasing the cathode electron current I_-. This can be seen by inspection of equation (4.12).

The sensitivity of this microengineered mass spectrometer device γ for xenon is obtained

$$\gamma = \frac{\text{ion current}}{\text{pressure}} = \frac{I_+}{P} = 9.656 \times 10^{18} \frac{I_- \sigma_{ion} l}{T} \quad \text{(A/Torr)}. \tag{4.22}$$

For the specific case of xenon, the sensitivity is

$$\gamma = \frac{I_{+min}}{P_{min\,Xe}} = \frac{10\text{fA}}{9.3 \times 10^{-12}\,\text{Torr}} \approx 1.08 \times 10^{-3}\,\text{A/Torr}.$$

Note that this sensitivity is independent of the minimum detectable ion current I_{+min}. The sensitivity for radon is even better. A specific value of sensitivity S for radon is not calculated because the literature does not indicate a value for radon cross section σ_{ion}.

CHAPTER FIVE
DEVICE PROCESSING

In this chapter the fabrication processing of the microengineered mass spectrometer is discussed This device consists of two chips. Chip A contains the electron cathode and the electron collector electrodes. Chip B contains the ion collectors. The cathode is a field emission vacuum microelectronics device. Thus this device is electron tunneling device for generating an ionizing electron emission into a vacuum. The ion collectors are coplanar electrodes.

5.1 Cathode Tips Array Fabrication Processing

The high ion-yield requires as high an electron current from the cathode as possible. It has been reported that the electron emission efficiency of a cone tips array is higher than that of wedge for the same area [9]. In this microengineered mass spectrometer device, an array of a large number of tips is chosen as the cathode. It is important that field emitters be very sharp since the electric field scales with sharpness and electron emission is strongly dependent on the electric field. Sharp emitters also make it possible for the device to operate at low voltage. The emitter damage by ion bombardment can be reduced at low operating voltage due to kinetic energy reduction, and therefore the emitter lifetime can be extended. Figure 5.1 is SEM micrograph of gated cone tip array.

Sharp field emitters can be produced in many ways. The emitters in this device are created by using an oxidation method for sharpening [11] [12]. During oxidation, the preliminary structure is sharpened due to the slower rate of surface reaction at the tip than at the sidewall. The faster surface reaction rate at the sidewall results in more silicon being consumed than at the tip and consequently the emitter is sharpened [13]. Only one mask level is needed for processing. Figure 5.2 shows the mask designed for cathode fabrication The major fabrication

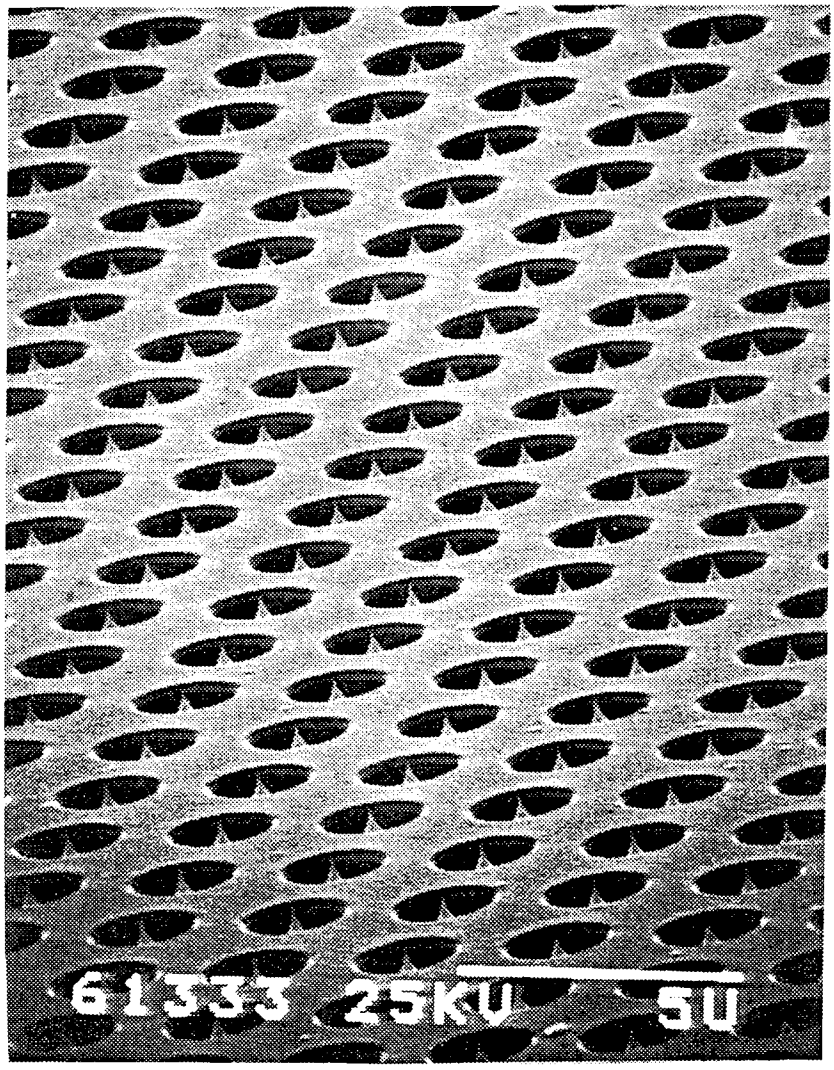

Figure 5.1 Cone-shaped emitter array with a 3-μm gate aperture [10].

steps are shown in Figure 5.3 (for simplicity, only one tip is indicated) and are described as follows [14]:

(a) Oxidize a silicon wafer to get a thermal oxide layer followed by spinning photoresist on the surface.

(b) Use lithography to transfer the pattern of mask into resist. The pattern for each tip is a square of 4μm by 4μm. Transfer photoresist pattern to silicon oxide and etch silicon (RIE preferred).

(c) Remove the photoresist and wet etch the silicon under a silicon mask

(d) Continue etching until the diameter of the silicon disc which supports the silicon oxide mask is decreased to around 100-200nm. This is done by controlling etch time.

(e) Remove the silicon oxide by HF.

(f) Oxidize and then remove silicon oxide by HF. This step may be repeated a few times to obtain an very sharp tips array. Final oxide stripping is done in HF which is used not only to remove the oxide but to passivate the silicon tips against further oxidation during the operation of the device.

After getting sharpened silicon tips array, the next step is to form the gate electrode which extracts the electrons emitted from the tips A self-aligned processing approach can be used [14]. The major steps are shown in Figure 5.4 and are described as follows:

(a) Obtain the silicon tips array by using the above mentioned method (figure 5.3).

(b) Form the first dielectric layer (dielectric I) which will control the gate opening. The diameter of gate opening is determined by the thickness of the dielectric on the sidewall. CVD silicon oxide can be used.

(c) Spin on the second dielectric layer (dielectric II), which planarizes the device surface.

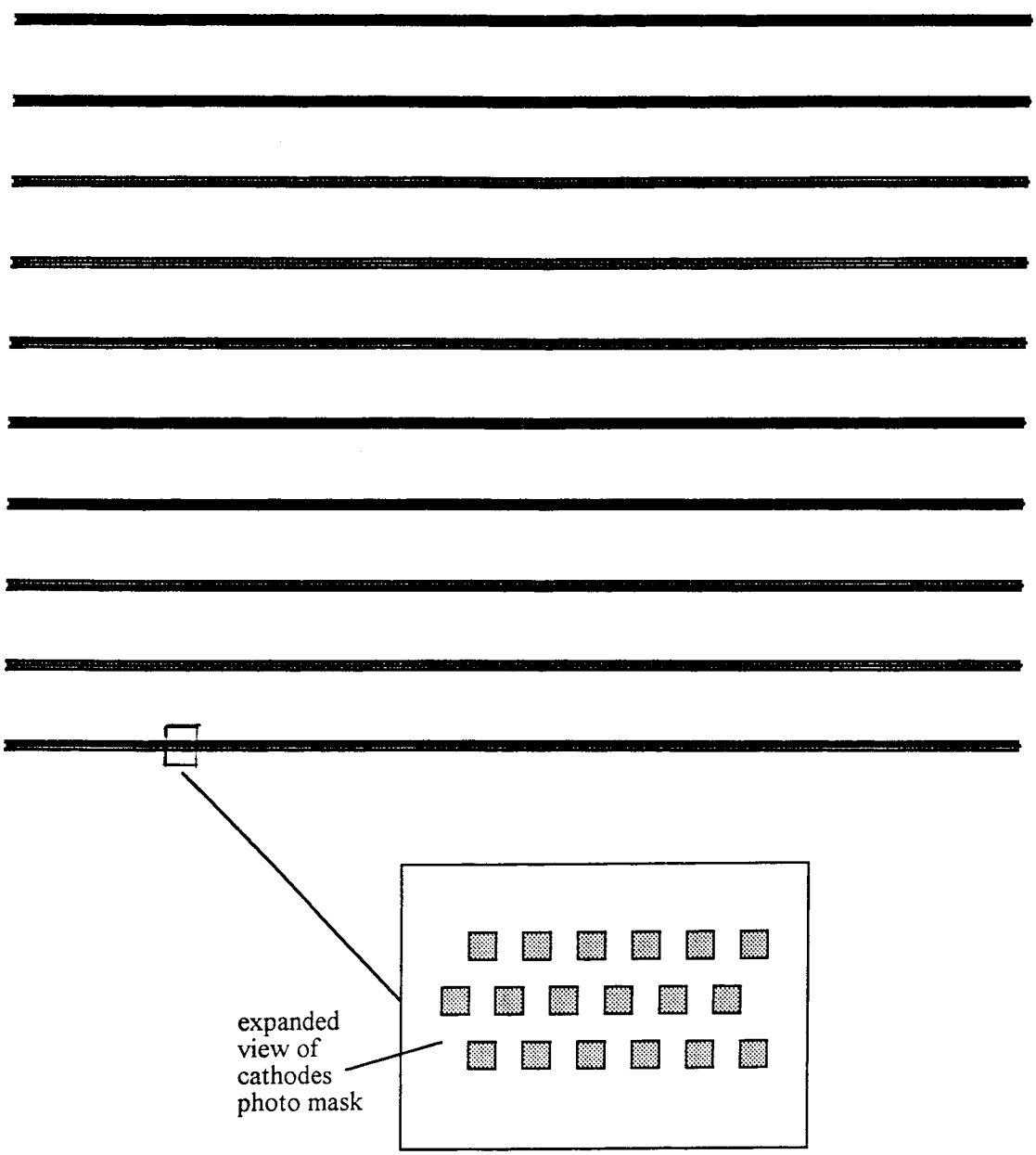

Figure 5.2 Photo mask for the electron cathode tip array.

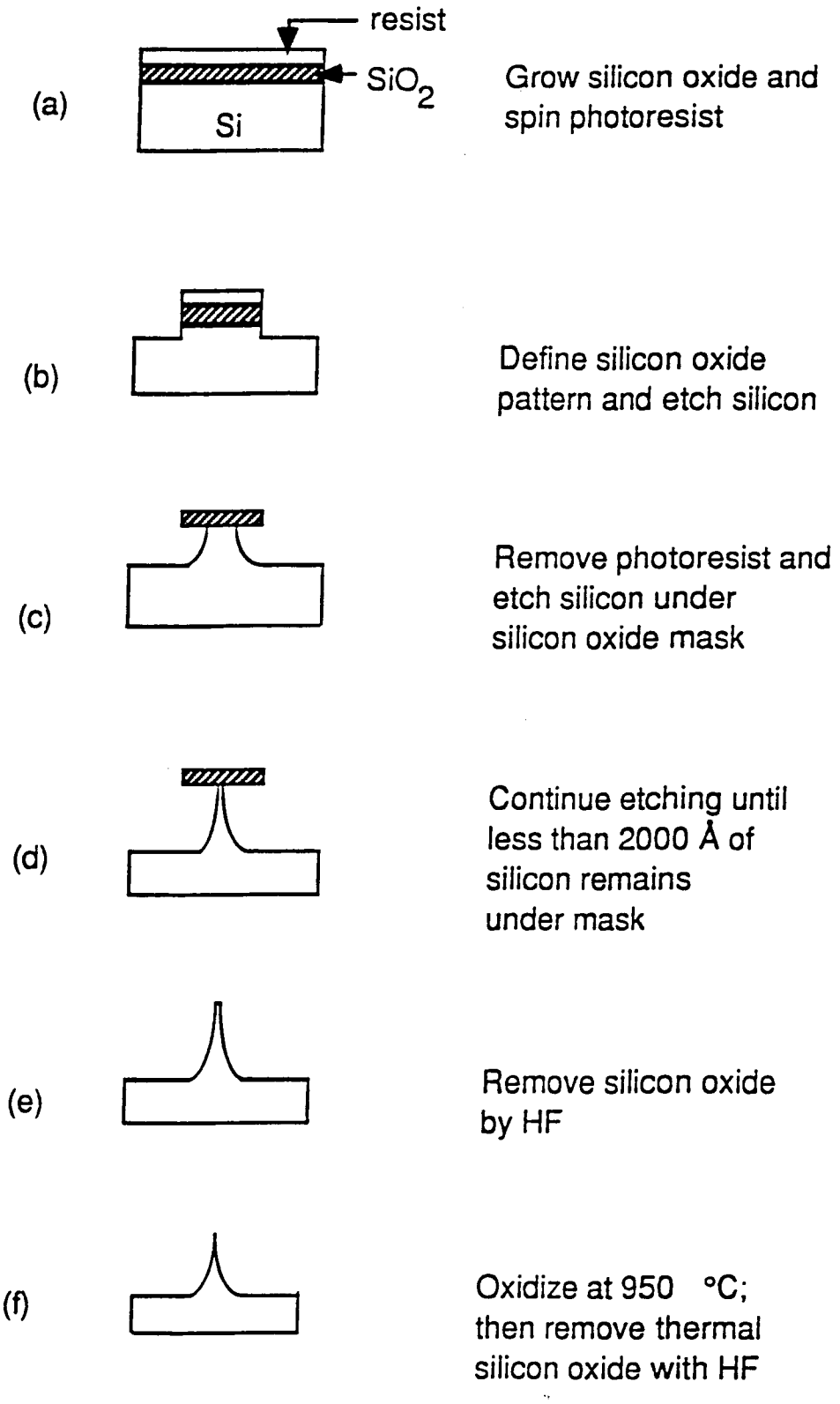

Figure 5.3 The major fabrication steps of atomically sharp silicon tip array

(d) Etch back dielectric II to a desired level which exposes dielectric I as required The dielectric II surface provides a planar substrate for the gate.

(e) Etch back dielectric I to form the gate opening and moreover to undercut the dielectric II layer, which enable the dielectric II to perform as a shadow mask for the following gate metal deposition. At this step dielectric II serves as an etching mask for dielectric I.

(f) Directionally deposit the gate metal (aluminum) with a desirable thickness. The dielectric II layer is used as a shadow mask during the gate metal deposition.

(g) Remove the gate metal from the tips. Since the gate metal is thinner on the tip than on the gate area due to the slope of the tip sidewall, controlled etching can be used to remove the gate metal from the tips while keeping gate metal on the gate area.

Using these procedures, we can obtain the array of cathode tips with gate electrode. The diameter of the gate opening is equal to 2t+d-2k, where t is the thickness of dielectric I at the sidewall of cathode tips, d is the diameter of the silicon cone at that height, and k is the thickness of the gate metal at the edge of dielectric II.

This process uses typical semiconductor processing technologies The main advantages of the method for forming the gate electrode are: (a) The gate is planar This helps to reduce capacitance between the gate and the cathode tips. (b) A small gate opening helps to increase electron emission. (c) A thick dielectric layer can be used between the gate and the cathode tips simultaneously with a small gate opening. This helps to maintain the necessary operating voltage and also to reduce capacitance between the gate an the cathode tips. (e) The gate opening is self-aligned to the tips. This puts the tip in the center of the gate opening without lithography and is termed a "self-aligned" process

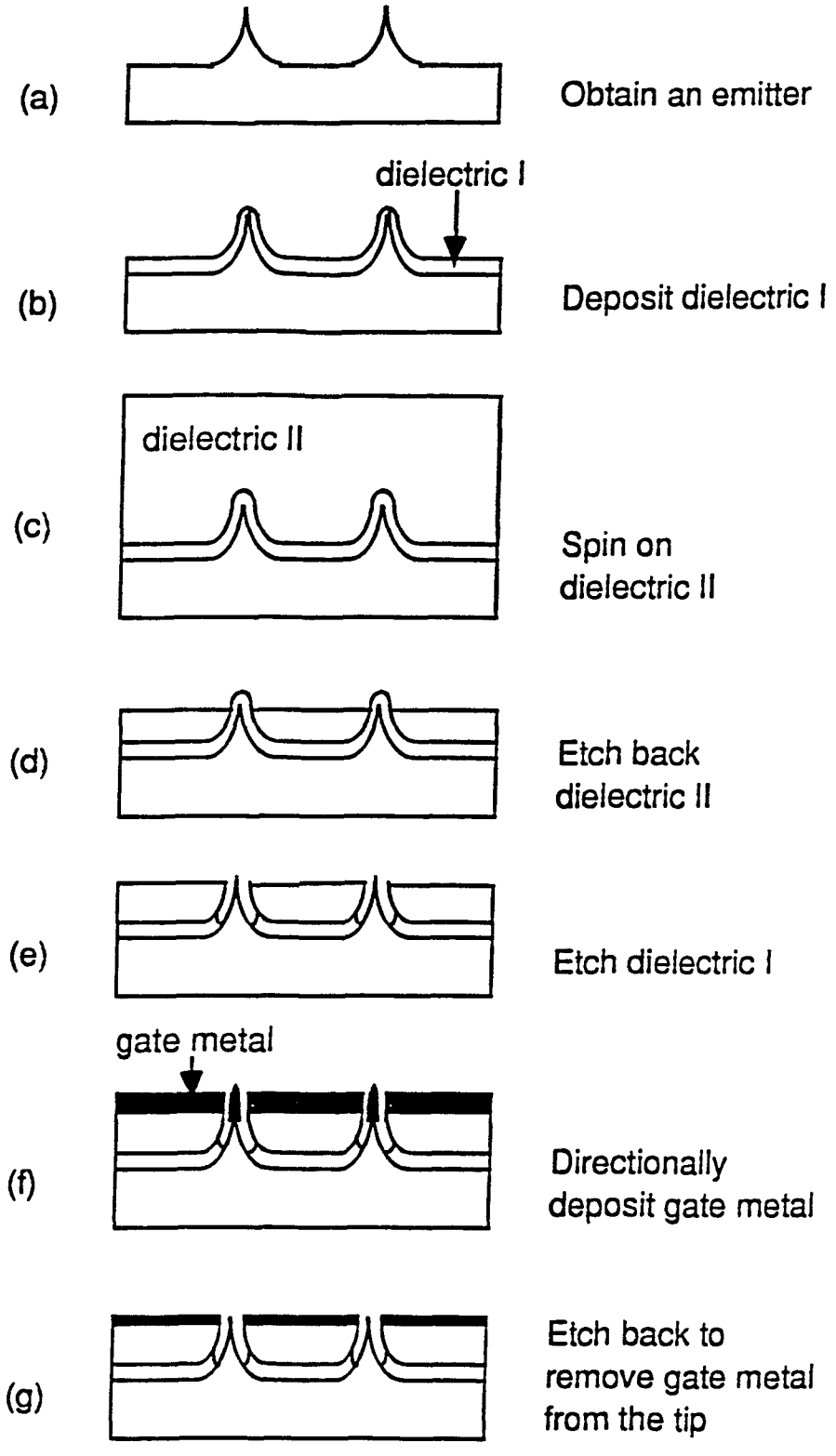

Figure 5.4 The major fabrication steps of self-aligned gate process

5.2 Ion Collector Electrode Processing

The major fabrication steps are shown in Figure 5.5 and are described as follows:

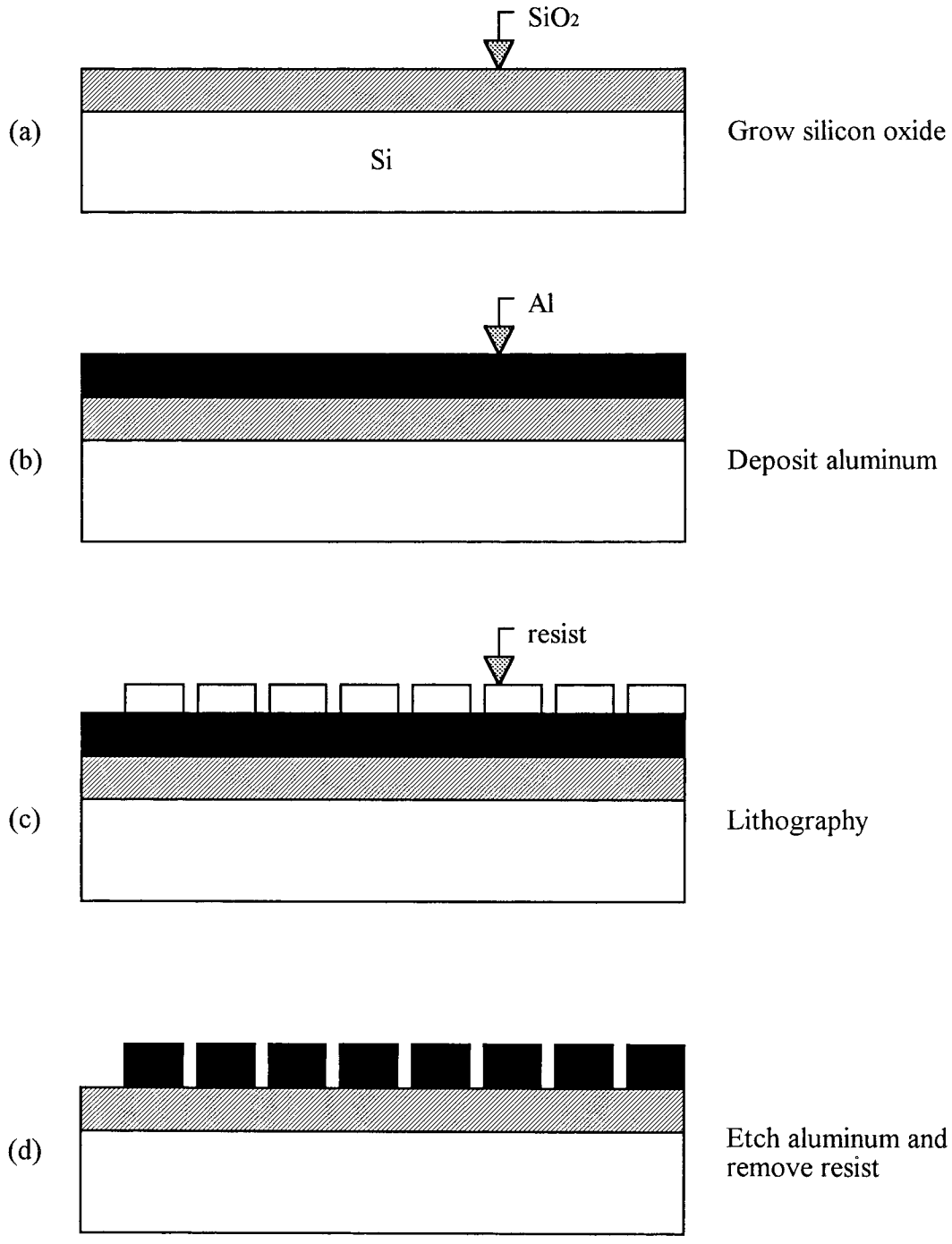

Figure 5.5 The major fabrication steps of coplanar ion collector

(a) Oxidize a silicon wafer to grow an oxide layer.

(b) Deposit (sputter) an aluminum layer.

(c) Spin photoresist on the aluminum surface and use lithography to transfer the electrode pattern into photoresist.

(d) Etch aluminum to form the electrode and remove photoresist.

5.3 Package Assembly

Chip A (contains array of cathode tips) and chip B (ion collectors) connected at a 90° angle as shown in Figure 5.6. An L-shaped metal preform (aluminum, copper, etc.) can be used as the base for the two chips. The chip A and B are bonded to the surface of the bent metal. Then it is mounted into a dual in-line DIP package with an internal ground plane.

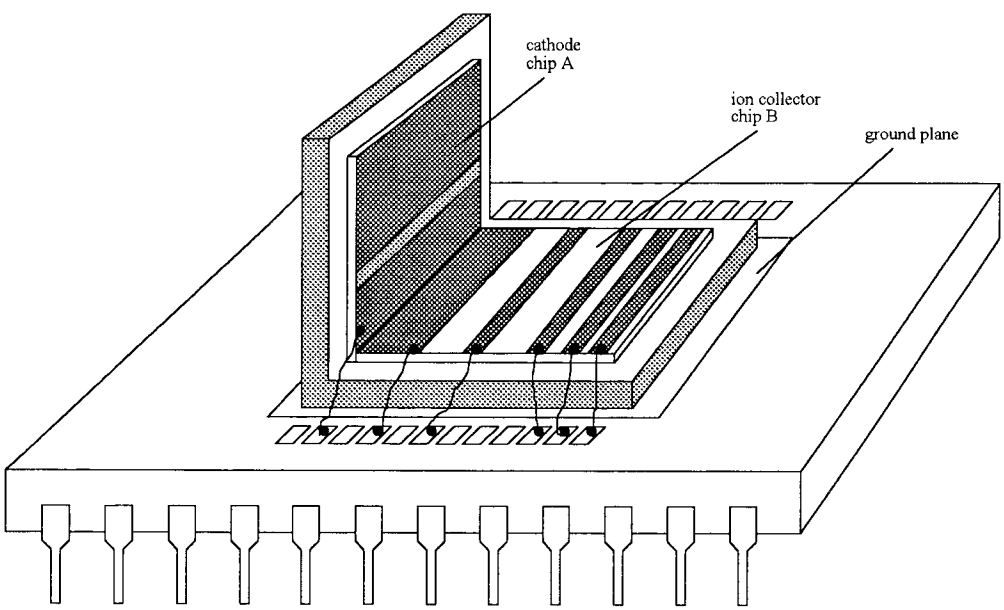

Figure 5.6 Assembled device in a 24-pin DIP package with ground plane

CHAPTER SIX
ENGINEERING TEST AND CHARACTERIZATION

This chapter describes the method to be used for testing the microengineered mass spectrometer device. The measurement circuit and environment (vacuum chamber) are presented.

6.1 Test Circuit

The test circuit for measuring the ion current vs gas pressure characteristics is shown in Figure 6.1. This circuit supplies a voltage to the gate electrode A series resistance R is used to limit the cathode current and protect the emitters somewhat from catastrophic breakdown. A voltmeter measures the supply voltage V. The total emitted electron current is measured by a microampere meter. The ion currents for different isotopes are measured by femtoampere meter through a switch.

6.2 Test Environment

The field emission device must work in the vacuum environment. A high vacuum system with electrical feedthrough is needed for device characterization. Figure 6.2 illustrates the high vacuum system that can be used for testing. A mechanical (roughing) pump is first used to evacuate the chamber to a medium vacuum range, then the high vacuum pump (diffusion pump) takes over and continues to evacuate the chamber to a high vacuum range. The test device is heated for outgasing. After the system pumps down to the desired vacuum level, the sample gas inlet valve is opened and the sample gas enters the vacuum chamber through a small orifice. For different kinds of sample gases, the ion current can be detected at different ion collectors.

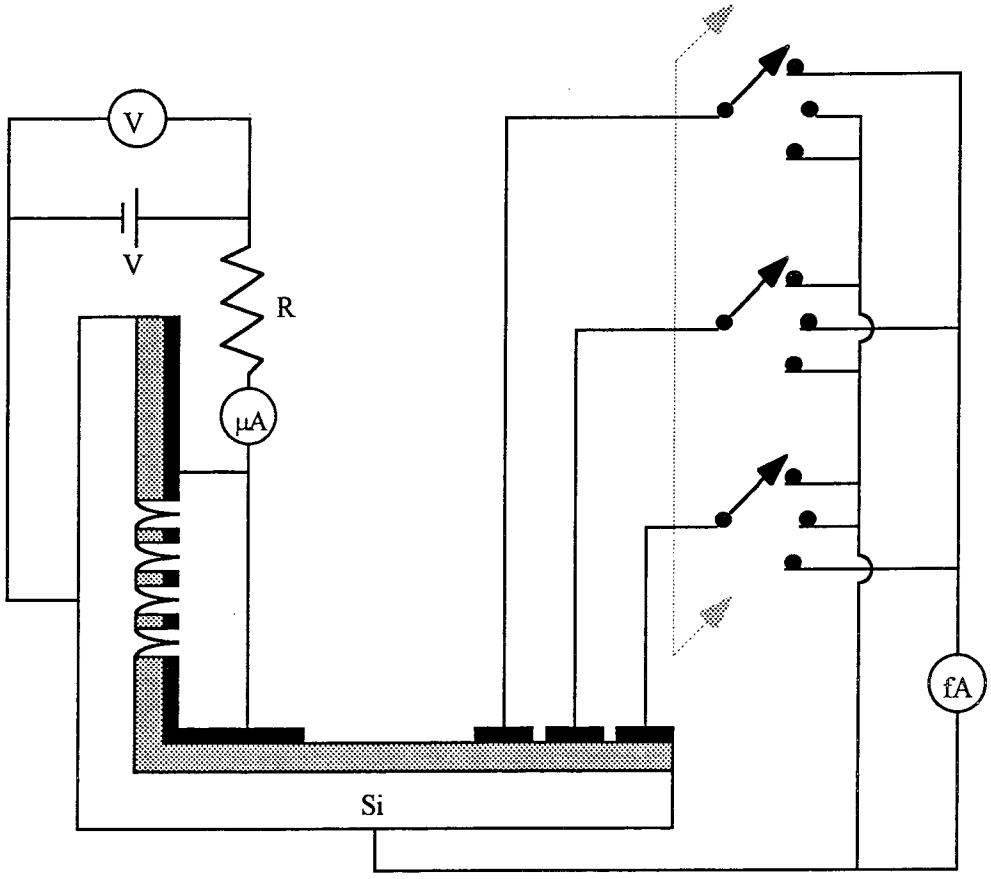

Figure 6.1 Test circuit.

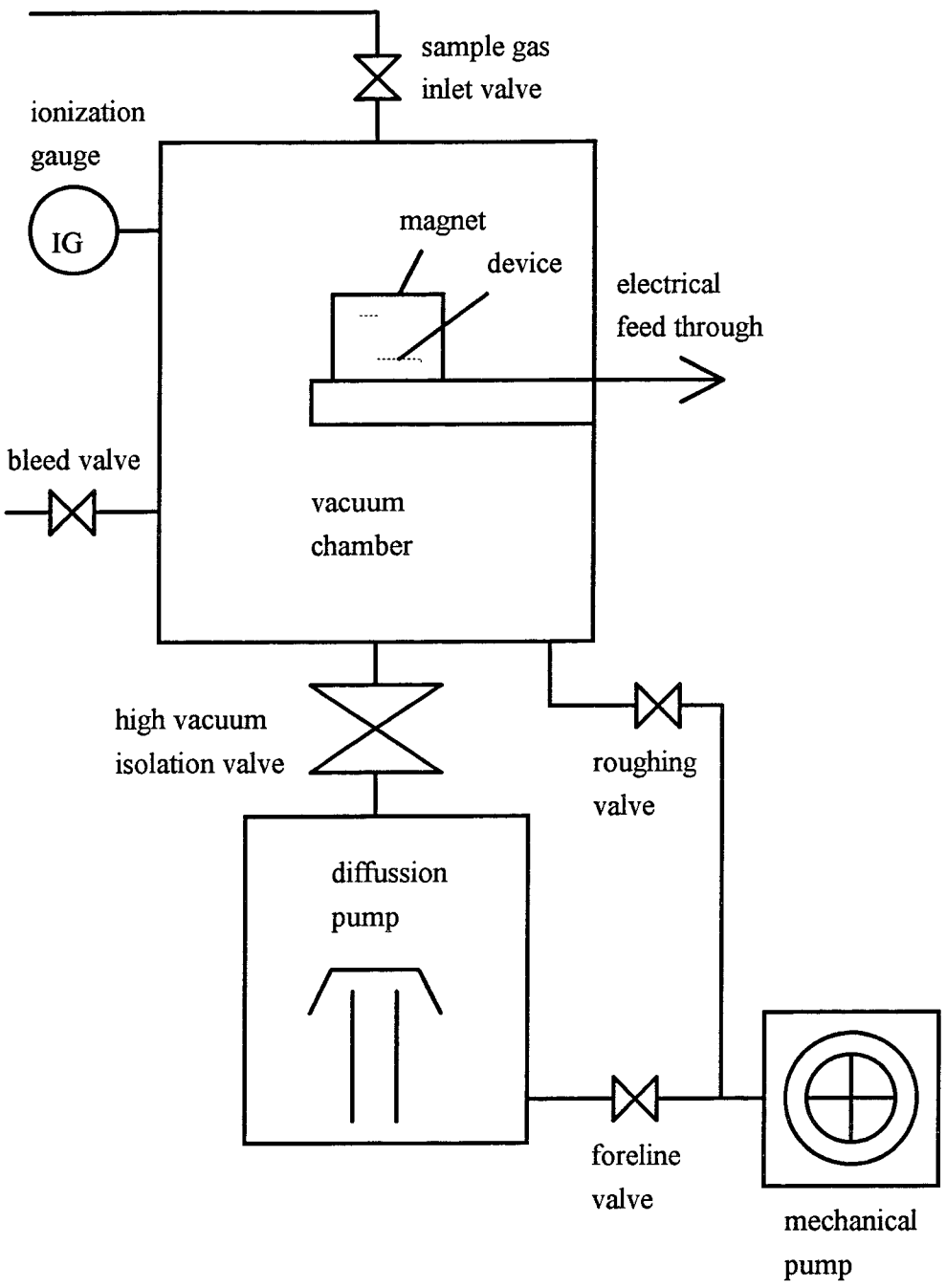

Figure 6.2 Schematic diagram of the high vacuum system used for testing the microengineered mass spectrometer.

6.3 Test Sample Gas

The desired test gases are hydrogen, helium, nitrogen, krypton, xenon, and radon. These kinds of gases can be tested respectively. Each kind of gas has its corresponding ion collector. This device can also detect oxygen, although some problem with oxidation of the cathode can occur. The testing time for oxygen must be short and partial pressure of oxygen must be very low. Radon is an important trace gas to detect for the environment assay application. This microengineered mass spectrometer can be used as a portable radon detector for environmental surveys. Since the radon emits α-ray (lifetime is 3.82 days) we cannot use it as test sample in our laboratory. Other heavy mass gases with a closely-spaced mass separation can be used. For testing the separation characteristic between xenon and radon we can instead use krypton and xenon. Since mass of Xe:mass of Rn (131:222) is very closed to mass of Kr:mass of Xe (84:131), if we detect Kr on Xe collector and Xe on Rn collector by increasing the gate voltage (ions get stronger repelling force and travel longer distance). Figure 6.3 is the simulation result. The gate voltage is raised to 84V from 50V, and the ion trajectories of Kr and Xe continue to be well separated. Figure 6.4 shows Xe and Rn trajectories for comparison (gate voltage is 50V).

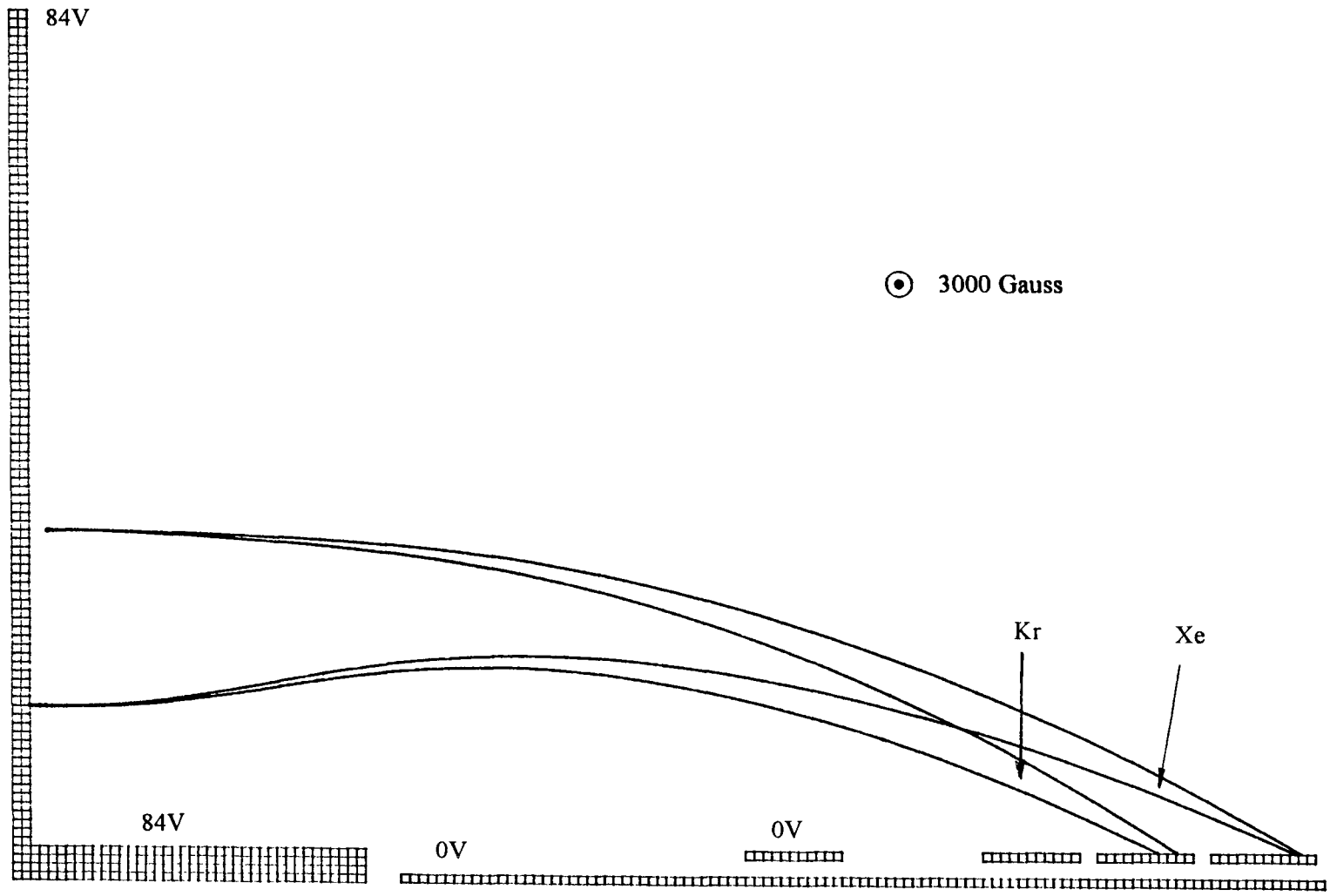

Figure 6.3 Ion trajectories of Kr^{84} and Xe^{131} collected at Xe and Rn collectors by increasing V to 84V. The ion collectors are maintained at near 0V. The scale unit is 0.1mm per square.

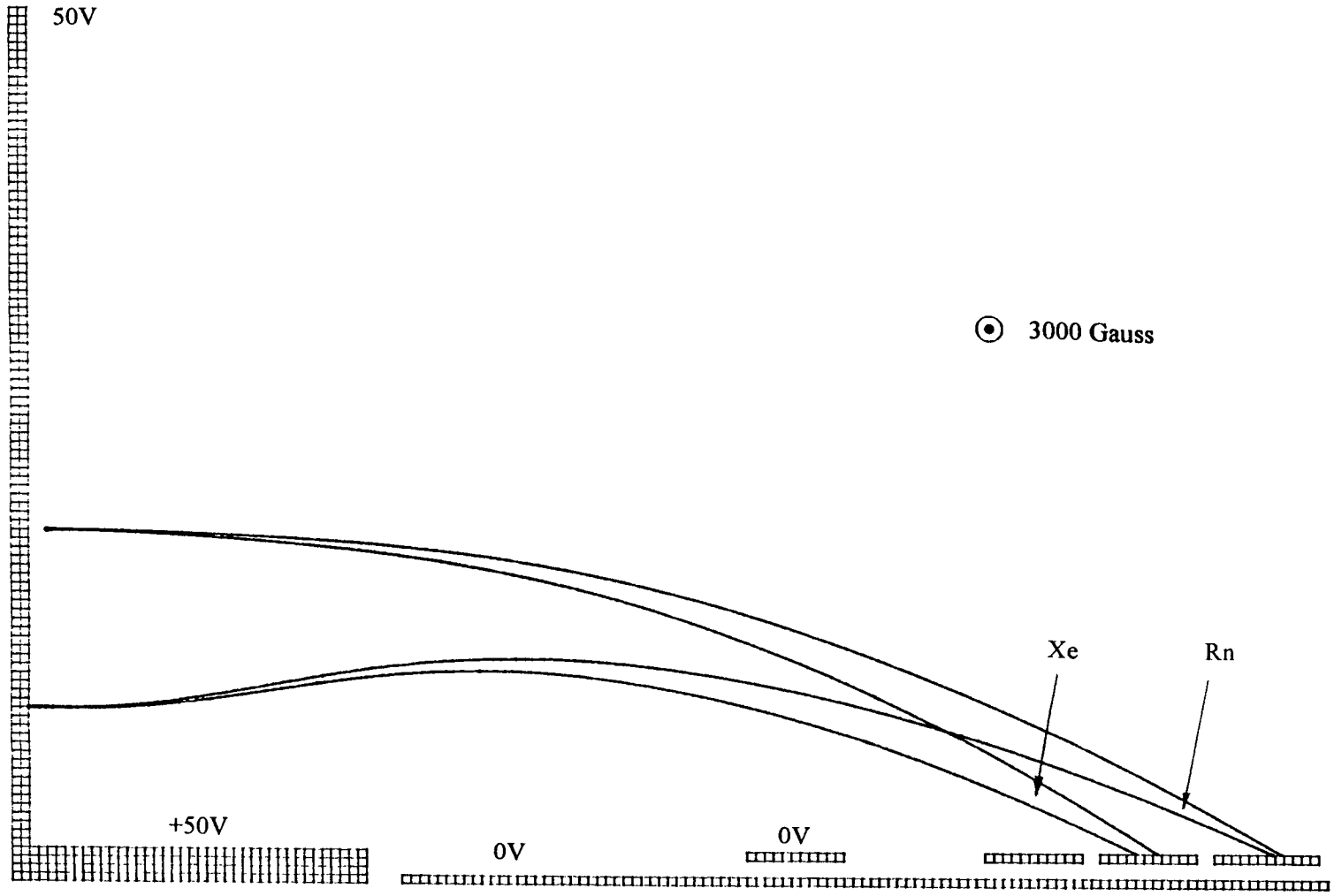

Figure 6.4 Ion trajectories of Xe^{131} and Rn^{222}. The ion collectors are maintained at near 0V. The units scale is 0.1mm per square.

CHAPTER SEVEN
CONCLUSIONS AND SUMMARY

It has been shown in this thesis that the microengineered mass spectrometer device could be made on silicon chips with dimension of about 1cm by 1cm. Several structures of the device have been simulated and discussed. The field emission cathode determines the sensitivity, the minimum detectable gas partial pressure, and the resolution. For the optimized structure (device III) the maximum detectable gas mass is 222 amu with the 3000 Gauss applied magnetic field. If the 7000 Gauss magnetic field is available, the dimension of this device can be reduced one third for the same maximum detectable gas mass. Calculation results shows the minimum detectable pressure is lower than 10^{-10} Torr which is in very high vacuum range. The minimum detectable pressure is proportional to the ionizing active volume. For most applications with partial pressure of interest in the range $\geq 10^{-7}$ Torr, this device has adequate minimum detectable level. The simulations show that the resolution is increased with decreasing ionizing active volume. If the active volume is made smaller (lower sensitivity), the mass resolution can be much higher. The sensitivity is independent of minimum detectable ion current I_{+min} and pressure P_{min} but is dependent of their ratio I_{+min}/P_{min}. This sensitivity represents the maximum sensitivity possible for a mass spectrometer without current limit.

This microengineered mass spectrometer has its own limitation. Due to the small dimension of the electrodes structure, the resolution is lower. The applied magnetic field must have high uniformity so that the ions trajectories can be precisely controlled and the resolution can also be improved. The cathode is a field emission device, its lifetime is reduced by oxidation or degradation of silicon tips. A high vacuum environment is needed for operating the device.

REFERENCES

[1] J. F. O'Hanlon, *A User's Guide to Vacuum Technology,* chapapter 8. John Wiley & Sons Inc., New York, 1989

[2] A. Roth, *Vacuum Technology,* chapter 1-3. North-Holland Publishing Company, Amsterdam, 1982.

[3] F. A. White, *Mass Spectrometry in Science and Technology.* John Wiley & Sons Inc., New York, 1968.

[4] L. Marton, *Advances in Electronics and Electron Physics.* Academic Press Inc., New York, 1956.

[5] D. A. Dahl and J. E. Delmore, *The SIMION User's Manual,* EG & G Idaho Inc., 1988.

[6] S. Wolf and R. N. Tauber, *Silicon Processing for the VLSI Era. Lattice Press, Sunset Beach, CA,* 1986

[7] Essam Nasser, *Fundamentals of Gaseous Ionization and Plasma Electronics,* chapter 3. Wiley-Interscience, New York, 1971.

[8] L. Zhang, A. Gui and W. N. Carr, "Lateral Vacuum Microelectronic Logic Gate Design". J. Micromech. Microeng., 1 , p.126, 1991

[9] W N. Carr, H. J. Wang and K. K. Chin, "Vacuum Microtriode Characteristics". J. Vac. Sci. Technol. A8(4), p 3581, 1990

[10] Keiichi Betsui, "Fabrication and Characteristics of Si Field Emitter Arrays". Technical Digest of the 4th IVMC, August 22-24, 1991, p 26, Nagahama, Japan.

[11] R. B. Marcus, T. S. Ravi, T. Gmitter, J. T Niccum, K. K. Chin, and D. Liu, "Atomically Sharp Silicon and Metal Field Emitters". IEEE Trans. Electron Devices, ED-38, p.2289, 1991.

[12] R. B. Marcus and T. T. Sheng, "The Oxidation of Shaped Silicon Surface". J Electronchem. Soc. Vol 129, No. 6, p 1278, 1982

[13] D B. Kao, J. P. McVittie, W. D. Nix, and K. C. Saraswat, "Two Dimensional Thermal Oxidation of Silicon-I. Experiments", IEEE Trans. Electron Devices, ED-34, p.1008, 1987.

[14] D. Liu, "Fabrication and Characterization of Gated Silicon Field Emission Micro Triodes". Dissertation, Dept. of E. E., NJIT, 1992.